Pion and Quark Masses Along the Chiral Critical Line in the $N_f = 2$ QCD Phase Diagram

Bachelor Thesis

Paul Frederik Depta

Institut für Theoretische Physik
Goethe-Universität Frankfurt am Main
September 2015

1st Supervisor: Prof. Dr. Owe Philipsen
2nd Supervisor: Prof. Dr. Marc Wagner
Advisor: Dr. Christopher Pinke

Contents

Abstract

The objective of this thesis is to calculate pion and quark masses in $N_f = 2$ lattice Quantum Chromodynamics (QCD) along the chiral critical line using Wilson fermions. This is done in order to relate results from lattice QCD simulations concerning the QCD phase diagram to physical quantities. More concretely, the results are needed in the investigation of the order of the chiral phase transition in the $N_f = 2$ chiral limit. This is part of current research in the Imaginary Chemical Potential Project in the working group of Professor Owe Philipsen, where the chiral critical line is mapped out. The pion and quark masses were determined using CL^{2}QCD, a lattice QCD program based on OpenCL. All statistical analyses were done with the Γ-method by Ulli Wolff.

Zusammenfassung

Ziel dieser Bachelorarbeit ist die Berechnung von Pion- und Quarkmassen in $N_f = 2$ Gitter Quantenchromodynamik (QCD) entlang der chiralen kritischen Linie mit Wilson Fermionen. Dies wird getan, um Ergebnisse von Gitter QCD-Studien über das QCD Phasendiagramm mit physikalischen Größen in Verbindung zu bringen. Konkreter werden die Resultate dieser Bachelorarbeit in der Untersuchung der Ordnung des chiralen Phasenübergangs im $N_f = 2$ chiralen Limes benötigt. Dies ist Gegenstand aktueller Forschung im Imaginären Chemischen Potential Projekt in der Arbeitsgruppe von Professor Owe Philipsen, wo die chirale kritische Linie numerisch vermessen wird. Die Pion- und Quarkmassen wurden mithilfe von CL^{2}QCD, einem auf OpenCL basierenden Gitter QCD Programm, bestimmt. Alle statistischen Analysen wurden mit der Γ-Methode von Ulli Wolff durchgeführt.

1. Introduction

In physics, four types of fundamental interactions have been established: the electromagnetic and the weak interaction, which may be unified to the electroweak interaction, the strong interaction and gravity. The strong interaction only dominates within scales of approximately 1 fm. The elementary particles of the strong interaction are quarks and the mediators, the gluons. There are six different quark flavors, all coming with quarks and antiquarks, and eight different gluons. The theory describing strong interaction is Quantum Chromodynamics (QCD). It does so by introducing a new charge, the color charge.

Due to gauge invariance only colorless objects can be observed in nature. Because of the strong interaction and the self-interaction of the gluons, which carry color charge themselves, quarks and gluons are never observed as free particles and are always confined into bound states (confinement). Only under extreme conditions strongly interacting matter undergoes a phase transition and forms a so-called Quark-Gluon-Plasma, in which quarks and gluons are quasi-free [cf. Pin14, p. v].

One possible way to form colorless objects are mesons. The most general definition of a meson is an object consisting of quarks and gluons and having a baryon number of 0, i.e. having exactly as many quarks as antiquarks. For the purpose of this thesis, it is sufficient to define mesons as particles consisting of a quark-antiquark pair. These attract each other by the exchange of gluons, which also leads to quark-antiquark creation and annihilation. Since quarks carry color, while antiquarks carry anti-color, correct combinations of these give colorless objects.

Mesons are classified using quantum numbers, i.e. spin, total angular momentum, parity, charge etc. The lightest mesons are pions. In nature, there are three different types of pions, charged pions $\pi^{\pm}$, which are anti-particles to each other and have a mass of 139.57018(35) MeV [Oli+14], and the neutral pion π^0 with a mass of 134.9766(6) MeV [Oli+14]. They consist of up- and down-quarks and -antiquarks. Another example of mesons consisting of these types quarks are ρ-mesons. It is worth noting that the attraction via gluon exchange may lead to quark-antiquark creation and annihilation with flavors different from up and down. Today, meson masses can in general be calculated using the theory of QCD only numerically using the so-called lattice formulation. In this thesis, pion and ρ-meson masses are determined, where the masses of ρ-mesons are only calculated for the purpose of scale setting, i.e. to express the pion masses in physical units and relate the results with "real world" QCD.

One might ask oneself what is meant by "real world" QCD. QCD is a theory with parameters being a priori free, i.e. parameters that can assume different values. In the real world, these parameters assume special values, at least in certain energy scales. This is referred to by "real world" QCD. Meson masses depend on these parameters and therefore, for different parameters, pions and ρ-mesons have different masses. An important point about this is that also the number of quark flavors and their masses may be chosen differently. The number of quark flavors can be chosen directly and is chosen to be

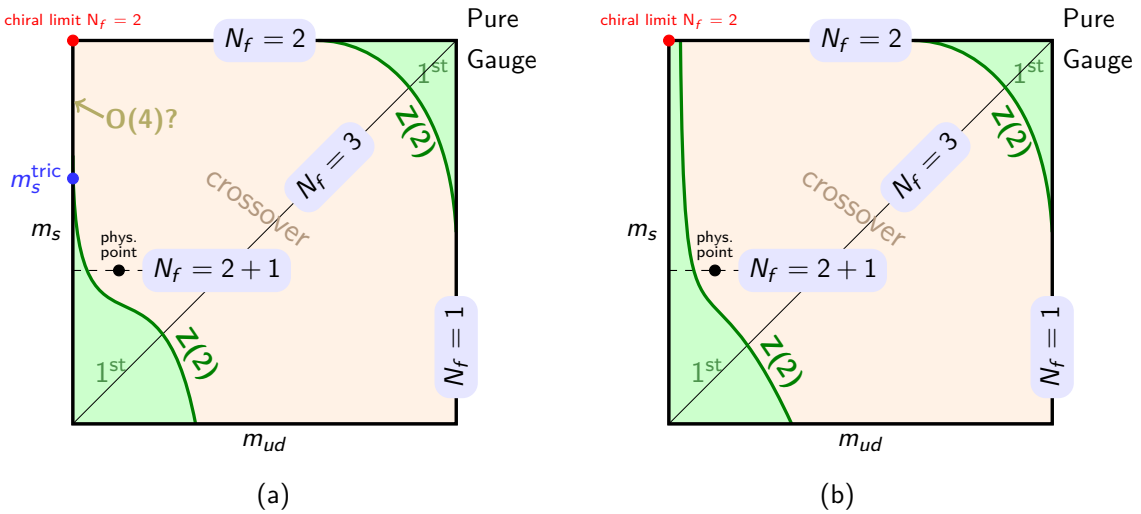

Figure 1.1.: (a) Columbia plot, (b) alternative Columbia plot for first order chiral phase transition at $N_f = 2$, $m_{u,d} = 0$, Fig. taken from [Pin14, p. 56].

$N_f = 2$ in this thesis. Since the up- and down-quarks are the lightest quarks, they may be identified by these two quark flavors. For technical reasons, these quarks (and antiquarks) are also assumed to have the same mass, which is a good approximation, since the mass of the next-heavier quark, the strange-quark, is approximately thirty times larger. However, only the bare quark mass is a direct input parameter for calculations and the renormalized quark mass has to be calculated. Since electroweak interactions are neglected in this thesis, having mass-degenerate two-flavor QCD means that all pions $\pi^{\pm}$ and π^0 have the same mass.

As the title says, the objective of this thesis is to calculate pion and quark masses along the chiral critical line in the $N_f = 2$ QCD phase diagram. This phase diagram is most commonly plotted with the temperature T against the chemical potential μ. It shows the different phases in which strongly interacting matter occurs. Its qualitative and quantitative features are not completely known. Experimentally, one can investigate the phase diagram in heavy ion collisions. Theoretically, it can be studied using lattice QCD (LQCD) simulations. The reason for calculating pion and quark masses in this thesis is to relate LQCD simulations concerning the chiral phase transition to physical parameters.

The chiral phase transition is the phase transition, in which chiral symmetry (cf. Sect. 2.3) is restored. The order parameter for this is the so-called chiral condensate $\langle\bar{\psi}\psi\rangle$. The knowledge of the chiral and deconfinement phase transitions at $\mu = 0$ for QCD with 3 flavors, i.e. u-, d- and s-quarks, where u- and d-quarks are mass-degenerate, is summarized in the so-called Columbia plot in Fig. 1.1. $N_f = 2$ means $m_{u,d} < \infty, m_s = \infty$, $N_f = 1$ means $m_{u,d} = \infty, m_s < \infty$, $N_f = 2+1$ means $m_{u,d} < \infty, m_s < \infty, m_{u,d} \neq m_s$, and $N_f = 3$ means $m_{u,d} = m_s < \infty$. Therefore, the $N_f = 2$ QCD phase diagram is only the top line in the Columbia plot. In this plot, the region of small quark masses on the left-hand side is connected to the chiral phase transition, whereas the region of heavy quark masses in the top right corner is related to the deconfinement transition. Between regions of first order phase transitions and regions of crossover transitions there are universality class $Z(2)$ critical lines, at which there are second order phase transitions. For example, the chiral critical line in the Columbia plot is the line which goes around the lower left corner. Note

that this is not the chiral critical line along which pion and quark masses are determined in this thesis. This critical line will be introduced below.

To this date, the order of the chiral phase transition in the $N_f = 2$ chiral limit $m_{u,d} = 0$, $m_s = \infty$ is not clear [cf. Pin14, pp. 55-58], [cf. PP15, p. 2]. For a temperature T smaller than the critical temperature T_c, chiral symmetry is broken spontaneously for vanishing light quark mass $m_{u,d} = 0$ and $\langle\bar{\psi}\psi\rangle \neq 0$. At $T > T_c$, chiral symmetry gets restored and $\langle\bar{\psi}\psi\rangle = 0$ [see Phi10, p. 17]. If $m_{u,d} > 0$, chiral symmetry is broken explicitly by the quark mass and $\langle\bar{\psi}\psi\rangle \neq 0$ for all temperatures T. There are two possible scenarios for the order of the chiral phase transition in the chiral limit at $\mu = 0$. Either it is of second order and most likely in the universality class $O(4)$ ((a) in Fig. 1.1) or there is a first order phase transition in the chiral limit ((b) in Fig. 1.1). In the first case, there is a crossover chiral transition for all $m_{u,d} > 0$, whereas in the second case, there is a first order chiral phase transition at low light quark masses $m_{u,d} < m_{u,d,c}$. At a certain light quark mass $m_{u,d,c}$ this region ends in a second order endpoint of universality class $Z(2)$ and for higher light quark masses $m_{u,d} > m_{u,d,c}$ there is a crossover chiral transition. The second order endpoint is also the endpoint at $m_s = \infty$ of the chiral critical line in (b) in Fig. 1.1. In terms of the pion mass the two scenarios can be found in Fig. 1.2.

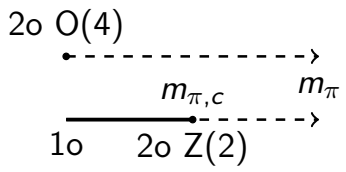

Figure 1.2.: Scenarios for $N_f = 2$ chiral phase transition, Fig. taken from [Pin14, p. 56].

The order of the chiral phase transition in the $N_f = 2$ QCD phase diagram is studied in the Imaginary Chemical Potential Project (IMuP) by Dr. Christopher Pinke and others in the working group of Professor Owe Philipsen. Their work has been published in [PP15]. Because of the so-called sign problem, which causes Monte Carlo algorithms (cf. Sect. 6.1) to fail at $\mu > 0$, simulations in the IMuP are performed at purely imaginary $\mu = i\mu_i \in \mathbb{C}$, $\mu_i \in \mathbb{R}$, and then, an analytical continuation in $(\mu/T)^2$ from $(\mu/T)^2 < 0$ to physical $(\mu/T)^2 > 0$ with $\mu > 0$ is performed, if needed. By doing so, one extends critical points from $\mu = 0$ to lines at imaginary μ. In the second scenario for the chiral phase transition ((b) in Fig. 1.1) this means that the $Z(2)$ second order endpoint becomes a $Z(2)$ second order critical line in a plot of $(\mu/T)^2$ against $m_{u,d}$. This is the chiral critical line along which pion and quark masses are calculated in this thesis. To the left of this line, i.e. at lower $m_{u,d}$, there is the first order region and to the right of this line, there is the crossover region. The critical line is the boundary between these regions. At $(\mu/T)^2 < (\mu^{\mathrm{RW}}/T)^2 = -\pi^2/9$, one has Roberge-Weiss endpoints, beyond which the phase diagram becomes periodic [cf. Pin14, pp. 85-89].

In previous LQCD studies, the critical value of the imaginary chemical potential $a\mu_c$, i.e. where the first order region terminates, has been determined for several values of the hopping parameter $\kappa := 1/(2am + 8)$, where a is the lattice spacing and m is the bare quark mass (before renormalization), using coarse lattices with temporal extensions $N_\tau = 4$. This is shown in Fig. 1.3. Note that because of $\kappa \propto 1/(am)$, the direction of the κ-axis is switched to agree with the previous description of the phase transition regions.

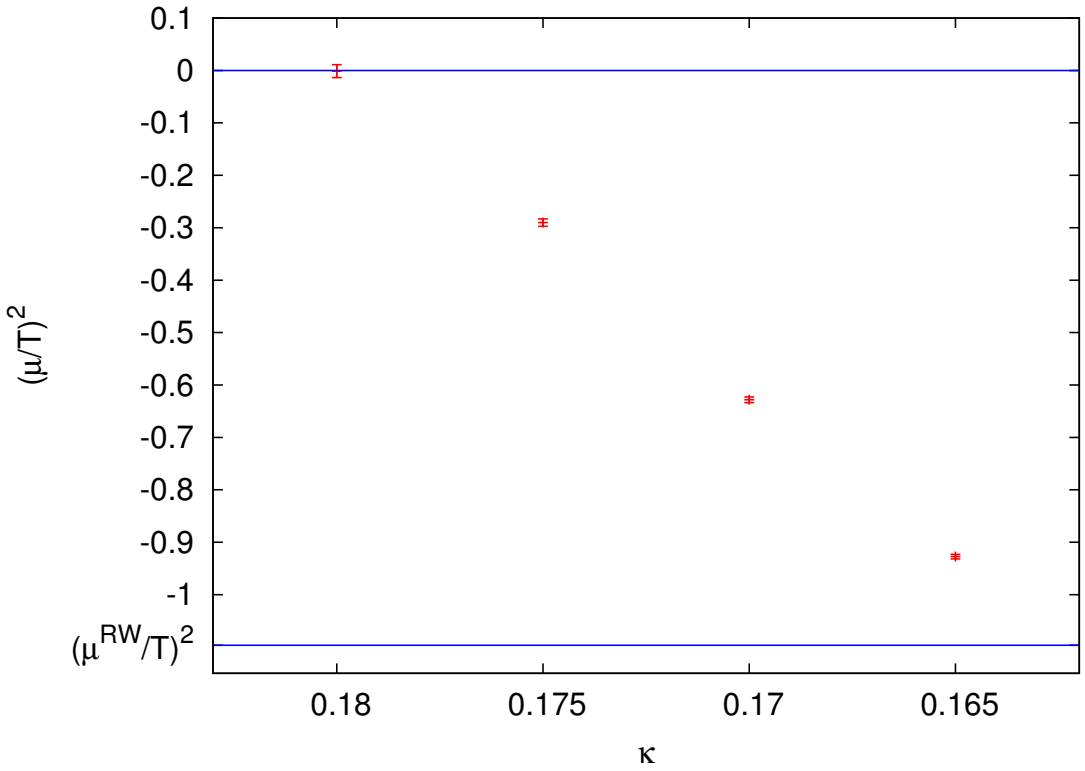

Figure 1.3.: Chiral critical line plot with $\kappa = 1/(2am + 8)$ as x-axis taken from [PP15, p. 4]. Note that $\mu_c/T = \mu_c a N_\tau$.

The objective of this thesis was then to use a physical parameter instead of the hopping parameter for the x-axis in the plot in Fig. 1.3. The quantities chosen for this are pion and quark masses, since pions are the lightest free particles bound by QCD. As it turned out in the course of this thesis, the chiral critical line still lies outside of the scaling region, which exists in the vicinity of tricritical points at low masses in the phase diagram [cf. PP15, p. 2]. Hence, quark masses are not determined for all points, as pion masses are sufficient for the scale setting. Note that even though the simulations on the phase diagram are performed at a temperature $T > 0$ and possibly an imaginary chemical potential, the simulations for the pion and quark masses are performed at $T = 0$ and $\mu = 0$, since they are zero temperature and zero density, i.e. zero chemical potential, parameters. The results for the pion masses from this thesis were used in [PP15] as a reference scale.

As in the studies by the IMuP, CL^{2}QCD[1], a lattice QCD program using OpenCL[2] developed by Dr. Matthias Bach, Dr. Christopher Pinke, and others, with Wilson fermions was used and extended for the simulations in this thesis. All statistical analyses were done using the Γ-method by Ulli Wolff [Wol04], whereas fits have been done using `gnuplot`[3]. All calculations in this thesis use natural units, where $\hbar = c = k_B = 1$. Furthermore, in computer simulations, all quantities have to be made dimensionless by a multiplication of an appropriate power of the lattice spacing. This is referred to by lattice units.

[1] `https://github.com/CL2QCD/cl2qcd`
[2] `https://www.khronos.org/opencl/`
[3] `http://www.gnuplot.info`

2. Theory

In this chapter, the fundamental theory for this thesis, QCD, is introduced. An overview of continuum QCD is given, which is then used to give an introduction to Lattice QCD. The last section of this chapter will present some details on chiral symmetry, which are needed for the calculation of quark masses in this thesis.

2.1. Continuum QCD

Quantum Chromodynamics can be defined via its action $S[\psi, \bar{\psi}, A]$, which has a fermionic part $S_F[\psi, \bar{\psi}, A]$ and a gluonic part $S_G[A]$. In Euclidean space, which can be obtained from Minkowski space with a Wick rotation and is suitable for a numerical implementation on a lattice, they read [see GL10, pp. 26-31]

$$S[\psi, \bar{\psi}, A] = S_F[\psi, \bar{\psi}, A] + S_G[A] \,, \tag{2.1}$$

$$S_F[\psi, \bar{\psi}, A] = \sum_{f=1}^{N_f} \int \mathrm{d}^4x \; \bar{\psi}^{(f)}(x) \left(\gamma_\mu (\partial_\mu + iA_\mu(x)) + m^{(f)} \right) \psi^{(f)}(x) \,, \tag{2.2}$$

$$S_G[A] = \frac{1}{2g^2} \int \mathrm{d}^4x \; \mathrm{tr}[F_{\mu\nu}(x) F_{\mu\nu}(x)] \,, \tag{2.3}$$

$$F_{\mu\nu}(x) = \partial_\mu A_\nu(x) - \partial_\nu A_\mu(x) + i[A_\mu(x), A_\nu(x)] \,, \tag{2.4}$$

where N_f is the number of flavors ($N_f = 2$ in the context of this thesis), x is a 4-dimensional space-time vector, and the Einstein summation convention is used. Note that there are only lower indices because all work in this thesis is done in Euclidean space. $m^{(f)}$ is the mass of the quark with flavor f, $\psi^{(f)}(x)$ and $\bar{\psi}^{(f)}(x)$ are the fermionic and anti-fermionic fields, and $A_\mu(x)$ are the gluon fields.

The fermionic part of the action can be derived by taking the Dirac action, requiring invariance under local SU(3) gauge transformations and doing a minimal substitution with the derivative becoming the covariant derivative [cf. GL10, pp. 26-31]:

$$\psi^{(f)}(x) \to \psi^{(f)\prime}(x) = \Omega(x)\psi^{(f)}(x) \,, \;\; \bar{\psi}^{(f)}(x) \to \bar{\psi}^{(f)\prime}(x) = \bar{\psi}^{(f)}(x)\Omega(x)^\dagger \,, \tag{2.5}$$

$$A_\mu(x) \to A'_\mu(x) = \Omega(x)A_\mu(x)\Omega(x)^\dagger + i(\partial_\mu \Omega(x))\Omega(x)^\dagger \,, \tag{2.6}$$

where $\Omega(x) \in \mathrm{SU}(3)$ for the complete context of this thesis. The gluonic part of the action then is the kinetic and self-interaction part for the gluon fields. This means that the fermionic fields become 3-dimensional vectors and the gauge fields become 3×3-matrices in the space the SU(3) transformations act on, the so-called color space. The corresponding indices are color indices. In total, the fermionic (spinor) fields have twelve components, resulting from four components in spin space and three components in color space (for each space-time direction). The gluon fields consist of four 3×3-matrices and they therefore have 36 components. In the following thesis, greek indices always refer to space-time or spin indices, while latin indices at objects with color components refer to their color indices. Note that both, matrix-vector and index notation, are used throughout this thesis,

but it is always clear in which notation an expression is.

In the continuum, a correlator is given by the path integral expression [cf. GL10, p. 18]

$$\langle 0|\,\hat{O}_2(\tau)\hat{O}_1(0)\,|0\rangle = \frac{1}{Z}\int \mathcal{D}[\psi,\bar{\psi}]\;\mathcal{D}[A]\;\mathrm{e}^{-S[\psi,\bar{\psi},A]}O_2[\psi(\tau),\bar{\psi}(\tau),A(\tau)]O_1[\psi(0),\bar{\psi}(0),A(0)]\;, \tag{2.7}$$

$$Z = \int \mathcal{D}[\psi,\bar{\psi}]\;\mathcal{D}[A]\;\mathrm{e}^{-S[\psi,\bar{\psi},A]}\;, \tag{2.8}$$

$$\mathcal{D}[\psi,\bar{\psi}] \coloneqq \prod_{x\in\mathbb{R}^4}\prod_{f,\alpha,c}\mathrm{d}\psi^{(f)}(x)_{\substack{\alpha\\c}}\;\mathrm{d}\bar{\psi}^{(f)}(x)_{\substack{\alpha\\c}},\;\mathcal{D}[A] \coloneqq \prod_{x\in\mathbb{R}^4}\prod_{\mu}\mathrm{d}A_\mu(x)\;. \tag{2.9}$$

$\hat{O}_2(\tau)$ and $\hat{O}_1(0)$ are operators, whereas $O_2[\psi(\tau),\bar{\psi}(\tau),A(t)]$ and $O_1[\psi(0),\bar{\psi}(0),A(0)]$ are functionals of the fields at all space coordinates, but only at euclidean time τ and 0 respectively. $|0\rangle$ is the vacuum of QCD and Z is the partition function of the system. An example for the operators are meson interpolators, where $\hat{O}_1(0) = \hat{O}^\dagger(0)$ creates a meson at euclidean time 0 and $\hat{O}_2(\tau) = \hat{O}(\tau)$ annihilates the meson at euclidean time τ. If one is able to calculate such a meson correlator, one can extract the meson mass out of it.

Since this expression cannot be solved exactly in general, the standard procedure in quantum field theory (QFT) is to evaluate this path integral using perturbation theory after gauge fixing, which has not been done yet. However, due to the running coupling in QCD, this procedure fails in QCD for small energies, since the contributions for the final expression do not get smaller with increasing order (one often says that the coupling is larger than 1). At high energies, one has asymptotic freedom with $g \to 0$ for the energy becoming infinite [cf. GL10, pp. 67-68], i.e. the strength of the strong interaction becomes less and less. Therefore, one needs to find another method to tackle a lot of problems with high coupling in QCD and a very powerful one for this is the lattice formulation.

2.2. Lattice QCD

The fundamental idea of Lattice QCD (LQCD) is to move from a continuous space-time to a discrete space-time. In order to be able to do calculations on a computer, one chooses a finite space-time with periodic boundary conditions. The lattice spacing is by convention called a and one uses the same lattice spacing for all spatial and temporal directions. All spatial extensions of the lattice are chosen to be the same with N lattice points in each spatial direction, whereas the temporal extension can be different with N_τ lattice points in the temporal direction. To summarize, the set of all lattice points is

$$\Lambda \coloneqq \{n \in \mathbb{Z}^4 \mid 0 \le n_i \le N_\sigma - 1\;\forall\; i = 1,2,3;\; 0 \le n_4 \le N_\tau - 1\}\;. \tag{2.10}$$

Whenever it appears in an expression, $\mathbf{n} = (n_1, n_2, n_3)$ is implied. Sometimes, n_4 is also referred to by n_τ.

The naive way to bring all expressions onto the lattice is by applying

$$x \in \mathbb{R}^4 \to an, n \in \Lambda\;, \tag{2.11}$$

$$\partial_\mu\psi(x) \to \frac{1}{2a}(\psi(an + a\hat{\mu}) - \psi(an - a\hat{\mu}))\;, \tag{2.12}$$

$$\int \mathrm{d}^4x \to a^4\sum_{n\in\Lambda}\;, \tag{2.13}$$

where $\hat{\mu}$ is the unit vector of $\mathbb{Z}^4$ in μ-direction. The derivative is chosen symmetrically for better convergence [cf. GL10, p. 19]. From now on, a is dropped in all dependences.

As described in [Pin14, p. 16], to move from continuum QCD to LQCD, the action has to have a form such that

$$S_{LQCD} = S_{QCD} + aS_1 + a^2 S_2 + \dots \ , \tag{2.14}$$

thus meaning that for $a \to 0$ continuum QCD is recovered and for finite a discretization errors, so-called lattice artifacts described by $S_1, S_2, \dots$, occur. This means that there are several possible ways to choose a lattice action, as long as they fulfill (2.14) and respect certain other requirements like gauge invariance. In the following two sections the discretizations chosen in this thesis are presented.

2.2.1. The Wilson Gauge Action

Keeping the gauge fields $A_\mu(x)$ on the lattice would mean breaking SU(3) gauge symmetry expicitly, which would produce meaningless results. Therefore, one has to introduce so-called link variables $U_\mu(n)$ "living" on the links between the lattice points (cf. Fig. 2.1), which are elements of SU(3) and transform in a gauge transformation according to [see GL10, p. 33]

$$U_\mu(n) \to U'_\mu(n) = \Omega(n) U_\mu(n) \Omega(n+\hat{\mu})^\dagger \ . \tag{2.15}$$

Define $U_{-\mu}(n)$ via [see GL10, pp. 33-34]

$$U_{-\mu}(n) \coloneqq U_\mu(n-\hat{\mu})^\dagger \ . \tag{2.16}$$

Together with (2.15) the transformation of $U_{-\mu}(n)$ under a SU(3) gauge transformation becomes

$$U_{-\mu}(n) \to U'_{-\mu}(n) = \Omega(n) U_{-\mu}(n) \Omega(n-\hat{\mu})^\dagger \ . \tag{2.17}$$

Since they have the same transformation, the link variables act as gauge-transporters in continuum QCD [see GL10, pp. 34-36]. Note that $U_\mu(n)$ are 3×3-matrices in color-space like $A_\mu(n)$.

In order to be able to build the gluonic (gauge) part of the action, a gauge-invariant quantity has to be found. The easiest way to construct such a quantity is to define the plaquette (cf. Fig. 2.1)

$$U_{\mu\nu}(n) \coloneqq U_\mu(n) U_\nu(n+\hat{\mu}) U_{-\mu}(n+\hat{\mu}+\hat{\nu}) U_{-\nu}(n+\hat{\nu}) \tag{2.18}$$

such that the trace of $U_{\mu\nu}(n)$ over the color indices is gauge invariant, which can be checked easily using (2.15), (2.16), (2.17) and the cyclicity of the trace. With this, a possible choice of the gauge action, the so-called Wilson gauge action, is [see GL10, p. 44]

$$S_G[U] = \frac{\beta}{3} \sum_{n \in \Lambda} \sum_{\mu<\nu} \mathrm{Re}\ \mathrm{tr}_c[\mathbb{1} - U_{\mu\nu}(n)] \ , \tag{2.19}$$

where

$$\beta = \frac{6}{g^2} \tag{2.20}$$

is the inverse coupling and tr_c is the trace over the color indices. It can be shown that the Wilson gauge action becomes the continuum gauge action for $a \to 0$ [see GL10, pp. 37-39]. The gauge invariance of the Wilson gauge action is obvious.

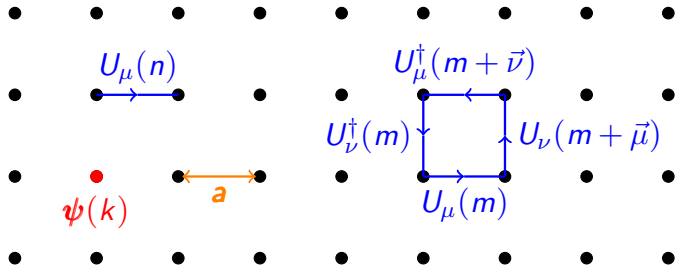

Figure 2.1.: Sketch of lattice quantities taken from [Pin14, p. 15], lattice spacing a, link variable $U_\mu(n)$, plaquette $U_{\mu\nu}(m)$ and fermionic fields $\psi(k)$.

2.2.2. The Wilson Fermion Action

The naive discretization of the fermionic action can be written as [see GL10, pp. 110-111]

$$S_F^0[\psi,\bar{\psi},U] = a^4 \sum_{f=1}^{N_f} \sum_{n,m\in\Lambda} \sum_{a,b,\alpha,\beta} \bar{\psi}^{(f)}(n)_{\underset{a}{\alpha}} D^{(f)}(n|m)_{\underset{ab}{\alpha\beta}} \psi^{(f)}(m)_{\underset{b}{\beta}} \,, \tag{2.21}$$

$$D^{(f)}(n|m)_{\underset{ab}{\alpha\beta}} = \sum_\mu (\gamma_\mu)_{\alpha\beta} \frac{U_\mu(n)_{ab}\delta_{n+\hat{\mu},m} - U_{-\mu}(n)_{ab}\delta_{n-\hat{\mu},m}}{2a} + m^{(f)}\delta_{\alpha\beta}\delta_{ab}\delta_{n,m} \,, \tag{2.22}$$

where $D^{(f)}(n|m)$ is the naive lattice Dirac operator and $\psi^{(f)}(n)$ are the fermionic fields "living" on the lattice points (cf. Fig. 2.1). As shown in [GL10, pp. 110-112] explicitly for the massless case, the inverse of the naive lattice dirac operator, the quark propagator, for free fermions has 16 poles for each fermion in contrast to only one pole in continuum QCD. These poles are so-called fermion doublers and have to be removed from the theory for meaningful calculations, since these fermion doublers do not even vanish in the continuum limit. One way to do so is with so-called Wilson fermions. They introduce a counterterm $\frac{4}{a}$ as an addition to the mass, which removes the doublers in the continuum limit. As a result, the Dirac operator and the fermionic part of the action become [see GL10, pp. 112-114]

$$D^{(f)}(n|m)_{\underset{ab}{\alpha\beta}} = \left(m^{(f)} + \frac{4}{a}\right)\delta_{\alpha\beta}\delta_{ab}\delta_{n,m} - \frac{1}{2a}\sum_{\mu=\pm1}^{\pm4} (\mathbb{1}-\gamma_\mu)_{\alpha\beta} U_\mu(n)_{ab}\delta_{n+\hat{\mu},m} \,, \tag{2.23}$$

$$S_F[\psi,\bar{\psi},U] = \sum_{f=1}^{N_f} a^4 \sum_{n,m\in\Lambda} \bar{\psi}^{(f)}(n) D^{(f)}(n|m)\psi^{(f)}(m) \,. \tag{2.24}$$

This particular choice is called the Wilson Dirac operator and the Wilson fermion action.

To simplify, define the hopping parameter

$$\kappa := \frac{1}{2(am+4)} \tag{2.25}$$

and rescale the fields via

$$\psi^{(f)}(n) \to a^2\sqrt{\frac{2a}{\kappa}}\,\psi^{(f)}(n) \,,\quad \bar{\psi}^{(f)}(n) \to a^2\sqrt{\frac{2a}{\kappa}}\,\bar{\psi}^{(f)}(n) \,, \tag{2.26}$$

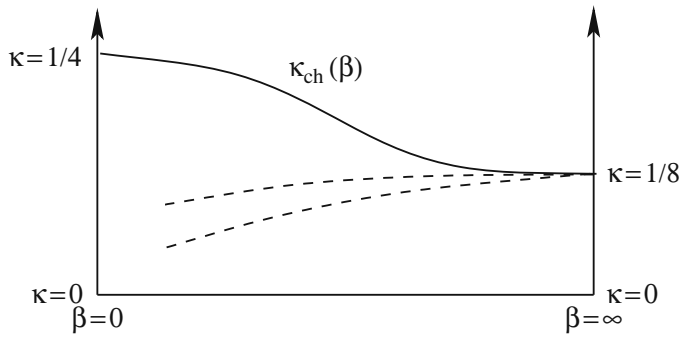

Figure 2.2.: Sketch of $\kappa_c(\beta) = \kappa_{ch}(\beta)$ taken from [GL10, p. 207]. Dashed curves have constant mass ratios, e.g. $m_\pi/m_\rho = \text{const}$ [cf. GL10, pp. 206-208].

such that [cf. GL10, pp. 114-115]

$$D^{(f)}(n|m)^{\alpha\beta}_{ab} = \delta_{\alpha\beta}\delta_{ab}\delta_{n,m} - \kappa \sum_{\mu=\pm1}^{\pm4} (\mathbb{1} - \gamma_\mu)_{\alpha\beta} U_\mu(n)_{ab} \delta_{n+\hat{\mu},m} \ , \tag{2.27}$$

$$S_F[\psi, \bar{\psi}, U] = \sum_{f=1}^{N_f} \sum_{n,m\in\Lambda} \bar{\psi}^{(f)}(n) D^{(f)}(n|m) \psi^{(f)}(m) \ . \tag{2.28}$$

Note that this rescaling differs from [GL10, pp. 114-115]. The rescaling here, however, gives dimensionless fields. Since $[S] = 1, [\psi] = [\bar{\psi}]$, and obviously, from (2.27), $[D] = 1$, one has $[\psi] = [\bar{\psi}] = 1$. This is going to be needed for the implementation in a computer program. Different discretizations include Staggered fermions, Domain Wall fermions, Wilson Clover fermions, and Wilson Twisted Mass fermions [see GL10, pp. 216-217, 243-260].

As stated in [Pin14, p. 18], the Wilson Dirac operator breaks chiral symmetry (cf. Sect. 2.3) explicitly, thus resulting in additive renormalization of the quark mass $m^{(f)}$. This means that the renormalized quark mass vanishes at the critical value $\kappa_c(\beta)$ of the hopping parameter, which does only equal the naive critical value $\kappa = 1/8$ for $\beta \to \infty$ [see Pin14, p. 18]. A sketch of $\kappa_c(\beta)$ can be found in Fig. 2.2. The quark mass with additive renormalization for a given $\kappa < \kappa_c$ becomes

$$am_q^{(f)}(\beta, \kappa) = \frac{1}{2}\left(\frac{1}{\kappa} - \frac{1}{\kappa_c(\beta)}\right) \ . \tag{2.29}$$

One can find the value for $\kappa_c(\beta)$ for a desired β by fitting literature values obtained by so-called chiral extrapolations. However, this leads to relatively large errors if there are not many values in the range of the desired β and it is therefore better to do the chiral extrapolations for the desired β anew.

At the end of this section, the formulae for charge conjugation $\mathcal{C}$ and parity transformation $\mathcal{P}$, under which the Wilson fermion action is invariant, are quoted and the formula for the γ_5-hermicity of the Wilson Dirac operator is given. They will be needed in the construction of meson interpolators in Sect. 3.1. All following formulae are taken from [GL10, pp. 117-121].

Charge conjugation is given by

$$\psi^{(f)}(n) \xrightarrow{\mathcal{C}} \psi^{(f)}(n)^{\mathcal{C}} = C^{-1}\bar{\psi}^{(f)}(n)^T \,,$$
$$\bar{\psi}^{(f)}(n) \xrightarrow{\mathcal{C}} \bar{\psi}^{(f)}(n)^{\mathcal{C}} = -\psi^{(f)}(n)^T C \,, \tag{2.30}$$
$$U_\mu(n) \xrightarrow{\mathcal{C}} U_\mu(n)^{\mathcal{C}} = U_\mu(n)^* \,, \tag{2.31}$$
$$\Rightarrow S_F[\psi,\bar{\psi},U] \xrightarrow{\mathcal{C}} S_F[\psi,\bar{\psi},U]^{\mathcal{C}} = S_F[\psi,\bar{\psi},U] \,, \tag{2.32}$$

where C is the charge conjugation matrix acting on space-time/spin indices, which is defined by

$$C\gamma_\mu C^{-1} = -\gamma_\mu^T,\ \mu = 1,\dots,4 \,. \tag{2.33}$$

With $\gamma_5 = \gamma_1\gamma_2\gamma_3\gamma_4$ one finds

$$\begin{aligned} C\gamma_5 C^{-1} &= C\gamma_1\gamma_2\gamma_3\gamma_4 C^{-1} = C\gamma_1 C^{-1} C\gamma_2 C^{-1} C\gamma_3 C^{-1} C\gamma_4 C^{-1} \\ &= \gamma_1^T\gamma_2^T\gamma_3^T\gamma_4^T = \gamma_4^T\gamma_3^T\gamma_2^T\gamma_1^T = \gamma_5^T \,, \end{aligned} \tag{2.34}$$

where the anti-commutation relations for the γ-matrices $\{\gamma_\mu,\gamma_\nu\} = 2\delta_{\mu\nu}\mathbb{1}_{4\times4}$ (A.2) have been used. Since in the Wilson gauge action the real part is taken and the charge conjugation affects only the imaginary part of the link variable's components, the Wilson gauge action is also invariant under charge conjugation.

Parity transformation is given by

$$\psi^{(f)}(\mathbf{n},n_\tau) \xrightarrow{\mathcal{P}} \psi^{(f)}(\mathbf{n},n_\tau)^{\mathcal{P}} = \gamma_4\psi^{(f)}(-\mathbf{n},n_\tau) \,,$$
$$\bar{\psi}^{(f)}(\mathbf{n},n_\tau) \xrightarrow{\mathcal{P}} \bar{\psi}^{(f)}(\mathbf{n},n_\tau)^{\mathcal{P}} = \bar{\psi}^{(f)}(-\mathbf{n},n_\tau)\gamma_4 \,, \tag{2.35}$$
$$U_i(\mathbf{n},n_\tau)(n) \xrightarrow{\mathcal{P}} U_i(\mathbf{n},n_\tau)^{\mathcal{P}} = U_i(-\mathbf{n}-\hat{i},n_\tau)^\dagger \,, i = 1,2,3 \,,$$
$$U_4(\mathbf{n},n_\tau)(n) \xrightarrow{\mathcal{P}} U_4(\mathbf{n},n_\tau)^{\mathcal{P}} = U_4(-\mathbf{n},n_\tau) \tag{2.36}$$
$$\Rightarrow S_F[\psi,\bar{\psi},U] \xrightarrow{\mathcal{P}} S_F[\psi,\bar{\psi},U]^{\mathcal{P}} = S_F[\psi,\bar{\psi},U] \,. \tag{2.37}$$

Again, the Wilson gauge action is also invariant under parity transformations [see GL10, p. 120].

γ_5-hermicity of the Wilson Dirac operator reads

$$D^\dagger = \gamma_5 D \gamma_5 \,. \tag{2.38}$$

Using A.3 to show that $\gamma_5 = \gamma_5^{-1}$, (2.38) implies

$$(D^{-1})^\dagger = \gamma_5 D^{-1} \gamma_5 \,. \tag{2.39}$$

2.2.3. The Lattice Path Integral

In analogy to the correlator in the continuum (2.7), the expression for a correlator in LQCD is [see GL10, pp. 39-41]

$$\begin{aligned} \langle O_2(n_\tau)O_1(0)\rangle = \frac{1}{Z}\int \mathcal{D}[\psi,\bar{\psi}]\ \mathcal{D}[U]\ \mathrm{e}^{-S_F[\psi,\bar{\psi},U]-S_G[U]} \\ O_2[\psi(n_\tau),\bar{\psi}(n_\tau),U(n_\tau)]O_1[\psi(0),\bar{\psi}(0),U(0)] \,, \end{aligned} \tag{2.40}$$
$$Z = \int \mathcal{D}[\psi,\bar{\psi}]\ \mathcal{D}[U]\ \mathrm{e}^{-S_F[\psi,\bar{\psi},U]-S_G[U]} \,, \tag{2.41}$$

where now

$$\mathcal{D}[\psi,\bar{\psi}] \coloneqq \prod_{n\in\Lambda}\prod_{f,\alpha,c} \mathrm{d}\psi^{(f)}(n)^{\alpha}_{c}\ \mathrm{d}\bar{\psi}^{(f)}(n)^{\alpha}_{c}\ ,\ \mathcal{D}[U] \coloneqq \prod_{n\in\Lambda}\prod_{\mu} \mathrm{d}U_{\mu}(x)\ , \tag{2.42}$$

such that for a finite lattice there is only a finite number of integration variables, which, of course, introduces discretization errors. Details on these errors and how the continuum is recovered can be found in [GL10, pp. 1-23] for the example of the Klein-Gordon field. Unless indicated otherwise, the expressions in this thesis have discretization and finite space-time errors implied. Note that the notation of the expectation value has been switched from inside a vacuum bra-ket to angular brackets.

The partition function Z has a direct correspondence to statistical mechanics [cf. Phi10, pp. 1-2, 10-11]:

$$Z = \mathrm{tr}\left[\mathrm{e}^{-\frac{\hat{H}}{T}}\right] = \mathrm{tr}\left[\mathrm{e}^{-N_\tau a\hat{H}}\right] = \sum_n \mathrm{e}^{-aN_\tau E_n}\ , \tag{2.43}$$

where $\hat{H}$ is the Hamilton operator and $T = \frac{1}{aN_\tau}$ is the temperature of the system, which is the inverse of the temporal extension of the system in physical units in Euclidean space, which is true for thermal field theory in general. $\{n\}$ is a complete set of eigenstates of $\hat{H}$ and E_n is the corresponding energy. Note that here, the chemical potential is $\mu = 0$. Since this thesis is about the determination of pion and quark masses, which are quantities that are determined at $T = 0$, all calculations have to be done for large N_τ, to be precise for $N_\tau \to \infty$ (such that in the continuum limit $a \to 0$ still $aN_\tau \to \infty$). An infinite temporal extension is, however, not possible on a computer, which means that one has to approximate it. As a rule of thumb, in order not to see any finite temperature effects, $N_\tau \approx 2N_\sigma, N_\tau \gg 1$ has to be used in simulations [cf. Pin14, p. 22]. For analytical calculations, however, the limit $N_\tau \to 0$ can be taken and these calculations can be used to find formulae to extract meson masses from correlators (cf. Sect. 3.2). Also, calculations at finite temperature have to be done using anti-periodic temporal boundary conditions for the fermionic fields and periodic temporal boundary conditions for the link variables (bosonic fields) [see Phi10, p. 11]. These boundary conditions are, however, not important for $T = 0$.

To calculate an expression like (2.40) one first splits up the expectation value in a fermionic and a gauge part [see GL10, pp. 103-104]. This can be done for any observable A, which may equal the correlator in (2.40), and reads

$$\langle A\rangle = \langle\langle A\rangle_F\rangle_G\ . \tag{2.44}$$

The fermionic part of the expectation value is

$$\langle A\rangle_F = \frac{1}{Z_F[U]}\int \mathcal{D}[\psi,\bar{\psi}]\ \mathrm{e}^{-S_F[\psi,\bar{\psi},U]}A[\psi,\bar{\psi},U]\ , \tag{2.45}$$

$$Z_F[U] = \int \mathcal{D}[\psi,\bar{\psi}]\ \mathrm{e}^{-S_F[\psi,\bar{\psi},U]}\ . \tag{2.46}$$

$Z_F[U]$ is the fermionic partition function, which will be evaluated further after the section on Wick's theorem. Since different flavors do not mix in the action, the fermionic expectation value factorizes in

$$\langle A\rangle_F = \prod_{f=1}^{N_f}\langle A\rangle_{(f)} \tag{2.47}$$

if

$$A[\psi,\bar{\psi},U]=\prod_{f=1}^{N_f}A^{(f)}[\psi^{(f)},\bar{\psi}^{(f)},U]\;, \tag{2.48}$$

where

$$\langle A\rangle_{(f)}=\frac{1}{Z_{(f)}[U]}\int\mathcal{D}[\psi^{(f)},\bar{\psi}^{(f)}]\;\mathrm{e}^{-\sum_{n,m\in\lambda}\bar{\psi}^{(f)}(n)D^{(f)}(n|m)\psi^{(f)}(m)}A^{(f)}[\psi^{(f)},\bar{\psi}^{(f)},U]\;, \tag{2.49}$$

$$\mathcal{D}[\psi^{(f)},\bar{\psi}^{(f)}]\coloneqq\prod_{n\in\Lambda}\prod_{\alpha,c}\mathrm{d}\psi^{(f)}(n)^{\alpha}_{c}\;\mathrm{d}\bar{\psi}^{(f)}(n)^{\alpha}_{c}\;, \tag{2.50}$$

and $A^{(f)}[\psi^{(f)},\bar{\psi}^{(f)},U]$ is a functional only of the spinors of quarks with flavor f.

The gauge part of the expectation value for any observable B, whose corresponding functional only depends on the link variables, is

$$\langle B\rangle_G=\frac{1}{Z}\int\mathcal{D}[U]\;\mathrm{e}^{-S_G[U]}Z_F[U]B[U]\;. \tag{2.51}$$

A standard procedure, and also the procedure used in this thesis, to calculate the correlator is to first calculate the fermionic part of the expectation value (2.45) analytically using Wick's theorem. Then, one creates gauge configurations using a hybrid Monte Carlo algorithm (cf. Sect. 4) with the appropriate probability distribution $\mathrm{e}^{-S_G[U]}Z_F[U]/Z$. By calculating the result for the fermionic part on the gauge configurations one finds an estimate of the gauge part of the expectation value (2.51) and thus the whole correlator.

Wick's Theorem

Fermions obey anti-commutation rules for all combinations of $f,f',n,n',\alpha,\alpha',a,a'$ [GL10, p. 105]:

$$\psi^{(f)}(n)^{\alpha}_{a}\psi^{(f')}(n')^{\alpha'}_{a'}=-\psi^{(f')}(n')^{\alpha'}_{a'}\psi^{(f)}(n)^{\alpha}_{a}\;, \tag{2.52}$$

$$\bar{\psi}^{(f)}(n)^{\alpha}_{a}\bar{\psi}^{(f')}(n')^{\alpha'}_{a'}=-\bar{\psi}^{(f')}(n')^{\alpha'}_{a'}\bar{\psi}^{(f)}(n)^{\alpha}_{a}\;, \tag{2.53}$$

$$\psi^{(f)}(n)^{\alpha}_{a}\bar{\psi}^{(f')}(n')^{\alpha'}_{a'}=-\bar{\psi}^{(f')}(n')^{\alpha'}_{a'}\psi^{(f)}(n)^{\alpha}_{a}\;. \tag{2.54}$$

In order to account for Fermi statistics, i.e. anti-commutation rules for fermions, fermions are represented by Grassmann numbers. The definition of a set of Grassmann number η_i, $i=1,2,\ldots,N$, is that

$$\eta_i\eta_j=-\eta_j\eta_i\;\forall\;i,j=1,2,\ldots,N\;. \tag{2.55}$$

One can also introduce a Grassmann algebra with $2N$ generators $\eta_i,\bar{\eta}_i$, $i=1,2,\ldots,N$, which all anti-commute with each other:

$$\eta_i\eta_j=-\eta_j\eta_i\;,\;\bar{\eta}_i\bar{\eta}_j=-\bar{\eta}_j\bar{\eta}_i\;,\;\eta_i\bar{\eta}_j=-\bar{\eta}_j\eta_i\;\forall\;i,j=1,2,\ldots,N\;. \tag{2.56}$$

This short definition is taken from [GL10, pp. 104-108], where more information on Grassmann numbers can be found.

For a gaussian integral with Grassmann numbers, there is the Matthews-Salam formula [see GL10, p. 108]

$$Z_F=\int\mathrm{d}\eta_N\mathrm{d}\bar{\eta}_N\;\ldots\;\mathrm{d}\eta_1\mathrm{d}\bar{\eta}_1\;\exp\left(\sum_{i,j=1}^{N}\bar{\eta}_iM_{ij}\eta_j\right)=\det[M]\;. \tag{2.57}$$

This formula can be generalized to Wick's theorem [see GL10, pp. 108-109]

$$\begin{aligned}\langle \eta_{i_1}\bar{\eta}_{j_1} \ \dots \ \eta_{i_n}\bar{\eta}_{j_n}\rangle_F &= \int \mathrm{d}\eta_N \mathrm{d}\bar{\eta}_N \ \dots \ \mathrm{d}\eta_1 \mathrm{d}\bar{\eta}_1 \ \eta_{i_1}\bar{\eta}_{j_1} \ \dots \ \eta_{i_n}\bar{\eta}_{j_n} \exp\left(\sum_{i,j=1}^{N} \bar{\eta}_i M_{ij} \eta_j\right) \\ &= (-1)^n \sum_{P(1,2,\dots,n)} \mathrm{sign}(P) (M^{-1})_{i_1 j_{P_1}} (M^{-1})_{i_2 j_{P_2}} \ \dots \ (M^{-1})_{i_n j_{P_n}} \ ,\end{aligned} \tag{2.58}$$

where P are permutations of $\{1, 2, \dots, n\}$ and $\mathrm{sign}(P)$ is the sign of the permutation.

As it is already written in the Matthews-Salam formula, Z_F can be computed by setting $M = -D$ and thus obtaining using (2.28)

$$Z_F = \prod_f \det[-D^{(f)}] \ . \tag{2.59}$$

Since this thesis works with two mass-degenerate quark-flavors (mass-degenerate up- and down-quark), one finds

$$Z_F = \det[D]^2 \ , \tag{2.60}$$

where $D = D^u = D^d$ is the (Wilson) Dirac operator for both flavors.

With Wick's theorem the fermionic expectation value of any product of fermion fields can be evaluated by setting $M = -D^u$ and using (2.28), e.g. [cf. GL10, p. 114]

$$\langle \psi^{(u)}(n)_{\substack{\alpha \\ a}} \psi^{(u)}(m)_{\substack{\beta \\ b}} \rangle_F = D_u^{-1}(n|m)_{\substack{\alpha\beta \\ ab}} \ , \tag{2.61}$$

where the flavor index has been moved down because of the index for the inverse. D^{-1} is called the quark propagator.

2.2.4. Scale Setting

As already stated in Sect. 2.2.2 for fields, quantities in a LQCD simulation on a computer must be dimensionless. Hence, all observables in the lattice formalism use lattice units with $\hbar = c = k_B = 1$ and the multiplication of an appropriate power of a to be dimensionless [see GL10, p. 63]. Therefore, a scale needs to be introduced to relate them to physical values. This means equating some observable to its physical value and then solving for a, which depends on the hopping parameter κ and the coupling β.

The first and easier, but rather crude method of setting the scale in this thesis is to calculate the pion and ρ-meson mass for given simulation parameters and then equating the mass of the ρ-meson to its physical value of 775.26(25) MeV [Oli+14]. However, this causes issues, since the ρ-meson mass in lattice and physical units depends on the simulation parameters. Besides, the pion mass in physical (natural) units in this scale setting is limited by the mass of the ρ-meson. Therefore, the scale setting can only be used as a rough estimate. However, when measuring the pion and ρ-meson masses one can compare the value of the ratio m_π/m_ρ, which is dimensionless and therefore does not directly need scale setting, to the physical value of $m_\pi/m_\rho = 0.180030(58)$, where the value of the mass of the charged pion $m_\pi = 139.57018(35)$ MeV [Oli+14] has been used.

The second and more precise method of scale setting is described in [Bor+12], where it was first presented, and involves calculating a quantity w_0, which is based on the Wilson flow. This way was only pursued for four simulations, since their results were directly needed by the IMuP. All other simulations were done only to extrapolate to the chiral limit to find $\kappa_c(\beta)$, for which a scale is not directly needed and therefore, the method via m_ρ together with the value of m_π/m_ρ is sufficient as an estimate. All calculations for the scale setting using w_0 have been done by Dr. Christopher Pinke, who then gave the results to the author of this thesis in order to be able to calculate the pion and quark masses in physical units.

2.3. Chiral Symmetry

The first part of this section works in continuum QCD with N_f flavors. Using vector notation for the flavors in the spinors $\psi = (\psi^{(f_1)}, \ldots, \psi^{(f_{N_f})})^T$, vector transformations

$$\psi \to \psi' = \mathrm{e}^{i\alpha T_i}\psi \,, \tag{2.62}$$

$$\psi \to \psi' = \mathrm{e}^{i\alpha \mathbb{1}}\psi \,, \tag{2.63}$$

and chiral or axial vector rotations

$$\psi \to \psi' = \mathrm{e}^{i\alpha\gamma_5 T_i}\psi \,, \tag{2.64}$$

$$\psi \to \psi' = \mathrm{e}^{i\alpha\gamma_5 \mathbb{1}}\psi \tag{2.65}$$

can be defined [see GL10, pp. 159-160], where T_i are the generators of the group $\mathrm{SU}(N_f)$. Note that the terms vector and axial vector transformations refer to the corresponding Noether currents, which are vector and axial vector currents with regard to Lorentz transformations [cf. GL10, pp. 159-160]. In fact, one could argue that (2.63) and (2.65) are no vector or axial vector transformations because spinors for different quark flavors do not mix with these transformations. However, in order to stay consistent with [GL10, pp. 159-160], the definitions above have been used here. The first vector transformation (2.62) is isospin symmetry generalized to N_f flavors and is a symmetry of the QCD action if the masses of all quarks are equal (degenerate). The second vector transformation (2.63) is a symmetry of the QCD action for arbitrary masses. The corresponding conserved quantity because of Noether's theorem is the baryon number. For $m^{(f)} = 0$, the chiral rotations (2.64) and (2.65) are a symmetry of the action of QCD. If all symmetries are realized, i.e. for $m^{(f)} = 0$, the total symmetry group of the QCD action reads [see GL10, pp. 159-160]

$$\mathrm{SU}(N_f)_L \times \mathrm{SU}(N_f)_R \times \mathrm{U}(1)_V \times \mathrm{U}(1)_A \,, \tag{2.66}$$

where the indices L and R refer to the left- and right-handed components, in which spinors can be splitted into. The indices V and A refer to the vector and axial vector Noether currents corresponding to (2.63) and (2.65). Chiral symmetry itself can be summarized by [see GL10, pp. 157-158]

$$\{\gamma_5, D\} = 0 \,, \tag{2.67}$$

where $D = \gamma_\mu(\partial_\mu + iA_\mu)$ is the massless Dirac operator in continuum QCD. The order parameter of chiral symmetry is the chiral condensate [see Pin14, pp. 10-11]

$$\langle\bar{\psi}\psi\rangle = \frac{T}{V}\frac{\partial \ln Z}{\partial m} \,, \tag{2.68}$$

where T is the temperature, V is the volume, Z is the partition function (2.43), and m is the fermion mass. For more than one flavor, the derivatives with respect to the masses add. In the following, QCD with two mass-degenerate flavors, i.e. $N_f = 2$, is always assumed. For this, the generators T_i can and are chosen to be the Pauli matrices (A.7), which are here referred to by $\tau^a, a = 1, 2, 3$.

Chiral symmetry is broken in several ways. The QCD vacuum breaks the symmetry $\mathrm{SU}(N_f)_L \times \mathrm{SU}(N_f)_R$ spontaneously [see Pin14, p. 11], even in the chiral limit. A finite quark mass breaks chiral symmetry explicitly. In addition, on a quantum level the fermion determinant is not invariant under the second axial vector rotation [see GL10, p. 160] and therefore, chiral symmetry is broken. The symmetry gets restored in the chiral phase transition. The fact that real world u- and d-quarks are light so that the explicit breaking of chiral symmetry is small [see GL10, p. 268] leads to an approximate realization of chiral symmetry in real world QCD. One can create partially conserved currents [see GL10, pp. 267-274]. For this, let

$$P^a \coloneqq \frac{1}{2}\bar{\psi}\gamma_5\tau^a\psi \,, \tag{2.69}$$

$$A^a_\mu \coloneqq \frac{1}{2}\bar{\psi}\gamma_\mu\gamma_5\tau^a\psi \,. \tag{2.70}$$

P^a is the pseudoscalar interpolator and A^a_μ is the axial vector interpolator [cf. GL10, p. 268].

The first relation, which will be used in this thesis, is the so-called partially conserved axial vector current (PCAC) relation [see GL10, p. 270]:

$$\partial_\mu \langle 0| A^{(r)a}_\mu(x) |\pi^b(\mathbf{p} = 0)\rangle = \delta_{ab} m_\pi^2 F_\pi e^{-M_\pi t} \,, \tag{2.71}$$

where $|\pi^b(\mathbf{p} = 0\rangle$ is a pion state, M_π is the pion mass, and F_π is the pion decay constant. The index (r) at the axial vector field indicates that it is the renormalized axial vector field.

Closely related to this relation is the so-called nonsinglet axial ward identity (AWI) [see GL10, pp. 272-173]

$$\partial_\mu A^{(r)a}_\mu = 2m^{(r)} P^{(r)a} \,, \tag{2.72}$$

where $m^{(r)}$ is the renormalized quark mass of the two mass-degenerate quarks. In Sect. 3.3, eqs. (2.71) and (2.72) will be used to calculate the correlator in order to be able to compute the so-called PCAC quark mass on the lattice.

The last relation, which comes from an expansion in small quark masses, is the so-called Gell-Mann-Oakes-Renner (GMOR) relation [see GL10, pp. 273-274]:

$$F_\pi^2 m_\pi^2 = -m^{(r)} N_f \Sigma^{(r)} + \mathcal{O}((m^{(r)})^2) = -2m^{(r)}\Sigma^{(r)} + \mathcal{O}((m^{(r)})^2) \,, \tag{2.73}$$

where $N_f = 2$ was plugged in and $\Sigma^{(r)}$ is the renormalized condensate. F_π, m_π, and $m^{(r)}$ are the same as before. This relation is only the leading term in $m^{(r)}$ and has possible corrections of $\mathcal{O}((m^{(r)})^2)$ [see GL10, p. 274], which are part of a systematic expansion in small quark masses leading to an effective theory, the so-called chiral perturbation theory. Note that also the PCAC relation and the AWI only hold for small quark masses.

2.3.1. Chiral Extrapolations

Using (2.29) and the GMOR relation (2.73) one finds for small pion and quark masses with the identification $m_q^{(f)}(\beta,\kappa) = m^{(r)}$ for QCD with two mass-degenerate quarks:

$$(am_\pi)^2 = -\frac{a\Sigma^{(r)}}{F_\pi^2} am^{(r)} + \mathcal{O}((m^{(r)})^2) = -\frac{a\Sigma^{(r)}}{F_\pi^2}\left(\frac{1}{\kappa} - \frac{1}{\kappa_c(\beta)}\right) + \mathcal{O}\left(\left(\frac{1}{\kappa} - \frac{1}{\kappa_c(\beta)}\right)^2\right). \tag{2.74}$$

This equation means that calculating $(am_\pi)^2$ constant β for several κ provides a possibility to determine $\kappa_c(\beta)$, which will be pursued in this thesis. Plotting $(am_\pi)^2$ against $1/\kappa$ and doing a linear fit in the range, where the GMOR relation can be applied, extrapolates to the value of $1/\kappa$, where $(am_\pi)^2 = 0$ implying $m^{(r)} = 0$. This value of κ is denoted $\kappa_{c,\pi}(\beta)$ (cf. Sect. 2.2.2). Note, however, that because of possible corrections of $\mathcal{O}((m^{(r)})^2)$, i.e. $\mathcal{O}((1/\kappa - 1/\kappa_c(\beta))^2)$, and because of the remaining a in the right-hand side of (2.74), there may be systematic uncertainties. One way to treat them is by using different linear fits and a quadratic fit to extrapolate to $(am_\pi)^2 = 0$ and using the difference of the results to give an error estimate.

According to [Iwa+96], κ_c can also be determined using an extrapolation in the PCAC quark mass, which is expected to give the same results for small N_f like in this thesis, since $N_f = 2$. This method directly exploits (2.29) by identifying $am_q^{(f)}(\beta,\kappa)$ with the PCAC quark mass. Therefore, the same extrapolation and determination of systematic errors as for $(am_\pi)^2$ for the PCAC quark mass also gives the critical value of the hopping parameter, here denoted by $\kappa_{c,q}(\beta)$. These extrapolations are so-called chiral extrapolations mentioned in Sect. 2.2.2 and their results can be used to calculate the renormalized quark mass at any κ at the same β (cf. (2.29)). Especially at high quark masses it is better to calculate the renormalized quark mass by a chiral extrapolation and not by directly using the PCAC quark mass.

3. Correlators

This chapter will detail the spectroscopic methods needed in this thesis. The first two sections will present the analytical calculations for the fermionic part of meson correlators (cf. (2.45)) and derive the formulae needed for the extraction of masses from meson correlators with the definition of the effective mass. The last section of this chapter will define the PCAC quark mass and present the analytical calculations for the fermionic path integral of the correlator needed for its calculation.

3.1. Meson Correlators

In general, meson correlators may be written as

$$\langle O(n_\tau)\bar{O}(0)\rangle \ , \tag{3.1}$$

where O and $\bar{O}$ are so-called meson interpolators. The corresponding operators $\hat{O}$ and $\hat{O}^\dagger$ annihilate and create mesons [cf. GL10, p. 124].

3.1.1. Non-Flavor-Neutral Mesons

At first, consider correlators of charged iso-triplet mesons (i.e. non-flavor-neutral mesons). For these mesons, the interpolator may be written as [cf. GL10, p. 125]

$$O(n) = \bar{\psi}^{(f_1)}(n)\Gamma\psi^{(f_2)}(n) \ . \tag{3.2}$$

$\psi^{(f_1)}(n)$ and $\psi^{(f_2)}(n)$ are spinors of flavors f_1 and f_2 respectively at the lattice position n, and Γ is a combination of Dirac-γ-matrices to obtain the quantum numbers of the desired meson. To obtain the full correlators, $\bar{O}(m)$ also needs to be found. Since $\bar{O}$ corresponds to $\hat{O}^\dagger$ and $O(n)$ corresponds to $\hat{O}$, it is obvious that

$$\left(\bar{\psi}^{(f_1)}(n)\Gamma\psi^{(f_2)}(n)\right)^\dagger = -\bar{\psi}^{(f_2)}(n)\gamma_4\Gamma^\dagger\gamma_4\psi^{(f_1)}(n) = \pm\bar{\psi}^{(f_2)}(n)\Gamma\psi^{(f_1)}(n) \tag{3.3}$$

$$\Rightarrow \bar{O}(m) = \bar{\psi}^{(f_2)}(m)\Gamma\psi^{(f_1)}(m) \ , \tag{3.4}$$

where $\gamma_4\Gamma^\dagger\gamma_4 = \pm\Gamma$ has been used and sign changes have been neglected because only the exponential decay is important for extracting meson masses [cf. GL10, p. 124]. Therefore, the fermionic parts of the expectation value of the meson correlators read

$$\langle O(n)\bar{O}(m)\rangle_F = \langle\bar{\psi}^{(f_1)}(n)\Gamma\psi^{(f_2)}(n)\bar{\psi}^{(f_2)}(m)\Gamma\psi^{(f_1)}(m)\rangle_F \ . \tag{3.5}$$

This expression can be modified further [cf. GL10, pp. 127-129]:

$$\begin{aligned}
\langle O(n)\bar{O}(m)\rangle_F &= \Gamma_{\alpha_1\beta_1}\Gamma_{\alpha_2\beta_2}\langle\bar{\psi}^{(f_1)}(n)^{\alpha_1}_{c_1}\psi^{(f_2)}(n)_{\beta_1}^{c_1}\bar{\psi}^{(f_2)}(m)^{\alpha_2}_{c_2}\psi^{(f_1)}(m)_{\beta_2}^{c_2}\rangle_F \\
&= -\Gamma_{\alpha_1\beta_1}\Gamma_{\alpha_2\beta_2}\langle\psi^{(f_2)}(n)_{\beta_1}^{c_1}\bar{\psi}^{(f_2)}(m)^{\alpha_2}_{c_2}\rangle_{(f_2)}\langle\psi^{(f_1)}(m)_{\beta_2}^{c_2}\bar{\psi}^{(f_1)}(n)^{\alpha_1}_{c_1}\rangle_{(f_1)} \\
&= -\Gamma_{\alpha_1\beta_1}\Gamma_{\alpha_2\beta_2}D^{-1}_{(f_1)}(n|m)^{\beta_1\alpha_2}_{c_1c_2}D^{-1}_{(f_2)}(m|n)^{\beta_2\alpha_1}_{c_2c_1} \\
&= -\mathrm{tr}\left[\Gamma D^{-1}_{(f_1)}(n|m)\Gamma D^{-1}_{(f_2)}(m|n)\right] \ .
\end{aligned} \tag{3.6}$$

The minus sign comes from the reordering of the Grassmann variables and (2.47) as well as Wick's theorem (2.58) have been used. Since this thesis works with mass-degenerate flavors $m^{(f_1)} = m^{(f_2)}$, one can use $D^{-1}_{(f_1)}(n|m) = D^{-1}_{(f_2)}(n|m) = D^{-1}(n|m)$. Note that the flavors f_1 and f_2 are identified with the lightest quarks, the u- and d-quarks. With γ_5-hermicity (2.39) and the cyclicity of the trace one finds

$$\langle O(n)\bar{O}(m)\rangle_F = -\mathrm{tr}\left[(D^{-1}(n|m))^\dagger \gamma_5 \Gamma D^{-1}(n|m)\Gamma\gamma_5\right] . \tag{3.7}$$

Since $\{\gamma_\mu, \gamma_5\} = 0$ (see (A.3)) and Γ is just a combination of γ-matrices, one has $\gamma_5\Gamma = \pm\Gamma\gamma_5$. Neglecting the possible sign change the result for the fermionic part of the expectation value of the correlator is

$$\langle O(n)\bar{O}(m)\rangle_F = -\mathrm{tr}\left[(D^{-1}(n|m))^\dagger \Gamma\gamma_5 D^{-1}(n|m)\Gamma\gamma_5\right] . \tag{3.8}$$

3.1.2. Flavor-Neutral Mesons

Until now, only non-flavor-neutral mesons have been considered. Now, flavor-neutral mesons described by an interpolator of the form

$$O(n) = \frac{1}{\sqrt{2}}\left(\bar{\psi}^{(f_1)}(n)\Gamma\psi^{(f_1)}(n) - \bar{\psi}^{(f_2)}(n)\Gamma\psi^{(f_2)}(n)\right), \tag{3.9}$$

$$\bar{O}(m) = \frac{1}{\sqrt{2}}\left(\bar{\psi}^{(f_1)}(m)\Gamma\psi^{(f_1)}(m) - \bar{\psi}^{(f_2)}(m)\Gamma\psi^{(f_2)}(m)\right) = O(m) , \tag{3.10}$$

will be considered. Corresponding to (3.5) one finds

$$\begin{aligned}
\langle O(n)\bar{O}(m)\rangle_F = \frac{1}{2}\langle &\left(\bar{\psi}^{(f_1)}(n)\Gamma\psi^{(f_1)}(n) - \bar{\psi}^{(f_2)}(n)\Gamma\psi^{(f_2)}(n)\right) \\
&\left(\bar{\psi}^{(f_1)}(m)\Gamma\psi^{(f_1)}(m) - \bar{\psi}^{(f_2)}(m)\Gamma\psi^{(f_2)}(m)\right)\rangle_F \\
= \frac{1}{2}(&\langle\bar{\psi}^{(f_1)}(n)\Gamma\psi^{(f_1)}(n)\bar{\psi}^{(f_1)}(m)\Gamma\psi^{(f_1)}(m)\rangle_F \\
&-\langle\bar{\psi}^{(f_1)}(n)\Gamma\psi^{(f_1)}(n)\bar{\psi}^{(f_2)}(m)\Gamma\psi^{(f_2)}(m)\rangle_F \\
&-\langle\bar{\psi}^{(f_2)}(n)\Gamma\psi^{(f_2)}(n)\bar{\psi}^{(f_1)}(m)\Gamma\psi^{(f_1)}(m)\rangle_F \\
&+\langle\bar{\psi}^{(f_2)}(n)\Gamma\psi^{(f_2)}(n)\bar{\psi}^{(f_2)}(m)\Gamma\psi^{(f_2)}(m)\rangle_F) .
\end{aligned} \tag{3.11}$$

Using the same procedure as for (3.6) for all expectation values, the fermionic part of the expectation value of the correlator becomes

$$\begin{aligned}
\langle O(n)\bar{O}(m)\rangle_F = \frac{1}{2}\Big(&\mathrm{tr}\left[\Gamma D^{-1}_{(f_1)}(n|n)\right]\mathrm{tr}\left[\Gamma D^{-1}_{(f_1)}(m|m)\right] - \mathrm{tr}\left[\Gamma D^{-1}_{(f_1)}(n|m)\Gamma D^{-1}_{(f_1)}(m|n)\right] \\
&-\mathrm{tr}\left[\Gamma D^{-1}_{(f_1)}(n|n)\right]\mathrm{tr}\left[\Gamma D^{-1}_{(f_2)}(m|m)\right] - \mathrm{tr}\left[\Gamma D^{-1}_{(f_2)}(n|n)\right]\mathrm{tr}\left[\Gamma D^{-1}_{(f_1)}(m|m)\right] \\
&+\mathrm{tr}\left[\Gamma D^{-1}_{(f_2)}(n|n)\right]\mathrm{tr}\left[\Gamma D^{-1}_{(f_2)}(m|m)\right] - \mathrm{tr}\left[\Gamma D^{-1}_{(f_2)}(n|m)\Gamma D^{-1}_{(f_2)}(m|n)\right]\Big) .
\end{aligned} \tag{3.12}$$

Again, since this thesis works with two mass-degenerate flavors, $D^{-1}_{(f_1)} = D^{-1}_{(f_2)} = D^{-1}$ can be applied. With γ_5-hermicity (2.39) and the cyclicity of the trace one finds

$$\langle O(n)\bar{O}(m)\rangle_F = -\mathrm{tr}\left[(D^{-1}(n|m))^\dagger \Gamma\gamma_5 D^{-1}(n|m)\Gamma\gamma_5\right] \tag{3.13}$$

as for non-flavor-neutral mesons.

3.1.3. Projection to Zero Momentum

For their final form, meson correlators first have to be projected to zero momentum via a Fourier transformation of the operator $O(n)$ [cf. GL10, pp. 332-333]. The other operator $\bar{O}(m)$ can be placed at the origin:

$$\tilde{O}(\boldsymbol{p}, n_\tau) = \frac{1}{N_\sigma^3} \sum_{n_1,n_2,n_3} O(\boldsymbol{n}, n_\tau) \mathrm{e}^{-\mathrm{i}a\boldsymbol{np}} \,, \tag{3.14}$$

$$\langle \tilde{O}(\boldsymbol{0}, n_\tau) \bar{O}(0) \rangle = \frac{1}{N_\sigma^3} \sum_{n_1,n_2,n_3} \langle O(\boldsymbol{n}, n_\tau) \bar{O}(0) \rangle \,, \tag{3.15}$$

where $\boldsymbol{p} = \boldsymbol{0}$ has been used in the second line and N_σ is the size of the lattice in each spatial direction as before. It is sufficient to only project one operator to zero momentum, since, using the Fourier components of $\bar{O}(m)$, only the one with zero momentum gives non-vanishing contribution because of the orthogonality of states with different momenta [see GL10, p. 131]. In fact, (3.15) holds for the fermionic as well as the gauge and the total part of the expectation value. Now, according to (2.44) the gauge part of the expectation value (2.51) has to be taken:

$$\begin{aligned} \langle \tilde{O}(\boldsymbol{0}, n_\tau) \bar{O}(0) \rangle =& \langle \langle \tilde{O}(\boldsymbol{0}, n_\tau) \bar{O}(0) \rangle_F \rangle_G \\ =& -\frac{1}{Z} \int \mathcal{D}[U] \mathrm{e}^{-S_G[U]} \det[D]^2 \\ & \frac{1}{N_\sigma^3} \sum_{n_1,n_2,n_3} \mathrm{tr} \left[(D^{-1}(\boldsymbol{n}, n_\tau | 0))^\dagger \Gamma \gamma_5 D^{-1}(\boldsymbol{n}, n_\tau | 0) \Gamma \gamma_5 \right] \,. \end{aligned} \tag{3.16}$$

Eq. (2.60) has been used for two mass-degenerate flavors. Now, a hybrid Monte Carlo algorithm can be used to estimate the complete meson correlator.

3.1.4. Obtaining Meson Quantum Numbers

As stated before, Γ is a combination of Dirac-γ-matrices to obtain the quantum numbers of the desired meson. In the following table a collection of Γ for different mesons can be found. Note that latin indices can always assume 1, 2 or 3 and γ_4 is used because all calculations are done in Euclidean time.

State	J^{PC}	Γ	Particles
Scalar	0^{++}	$\mathbb{1},\ \gamma_4$	$f_0,\ a_0,\ K_0^*,\ \ldots$
Pseudoscalar	0^{-+}	$\gamma_5,\ \gamma_4\gamma_5$	$\pi^\pm,\ \pi^0,\ \eta,\ K^p m,\ K^0,\ \ldots$
Vector	1^{--}	$\gamma_i,\ \gamma_4\gamma_i$	$\rho^\pm,\ \rho^0,\ \omega,\ K^*,\ \phi,\ \ldots$
Axial vector	1^{++}	$\gamma_i\gamma_5$	$a_1,\ f_1,\ \ldots$
Tensor	1^{+-}	$\gamma_i\gamma_j$	$h_1,\ b_1,\ \ldots$

Table 3.1.: Table from [GL10, p. 126]. Γ for the most important meson interpolators, J is the total angular momentum, P is parity and C is charge conjugation, where the classification using C is for flavor-neutral interpolators only.

In CL^{2}QCD, which was used for this thesis, meson correlators for twisted mass fermions had already been implemented at the beginning of this thesis. The correlators for twisted mass and Wilson fermions have the same structure if Γ consists of an even number of

γ-matrices different from γ_5 [cf. Pin14, p. 24]. Therefore, $\Gamma = \gamma_5$ for pseudoscalar and $\Gamma = \gamma_4\gamma_i$ for vector mesons were used being already implemented. For correlators with free indices the result for each index as well as the average is given as output by CL^{2}QCD.

3.1.5. Point Sources

As stated in [GL10, pp. 135-136], the full propagator D^{-1} is not sparse and consists of $\mathcal{O}(10^{12})$ complex numbers even though the Dirac operator D may have many vanishing entries. Therefore, calculating with the complete propagator is not economical and one has to introduce quark sources. The easiest way to do so is using point sources. Since each entry $D^{-1}(n|m)^{\alpha\beta}_{ab}$ connects a source point (m, β, b) with a sink point (n, α, a), one column of the propagator can be considered, i.e. just the parts from a fixed set of (m_0, β_0, b_0) [cf. GL10, pp. 135-136]. This gives

$$D^{-1}(n|m_0)_{\substack{\alpha\beta_0\\ab_0}} = \sum_{m,\beta,b} D^{-1}(n|m)_{\substack{\alpha\beta\\ab}} S_0^{(m_0,\beta_0,b_0)}(m)_{\substack{\beta\\b}} \,, \tag{3.17}$$

where point sources

$$S_0^{(m_0,\beta_0,b_0)}(m)_{\substack{\beta\\b}} \coloneqq \delta_{mm_0}\delta_{\beta\beta_0}\delta_{bb_0} \tag{3.18}$$

have been introduced. The source m_0 can be placed at the origin. When using point sources, the correlators have to be evaluated for 12 sources, i.e. for all combinations of (β_0, b_0) [cf. GL10, pp. 136-136].

In all of the following calculations, the source will be placed at 0. However, it is better to use randomly placed sources in simulations. In order to average out fluctuations, the correlators were calculated for eight different random positions for the source for each gauge configuration in all simulations in this thesis. The temporal positions on the lattices in these calculations then got shifted such that $m_\tau = (m_0)_\tau = 0$ and n_τ is the temporal distance between the source and the sink. After doing so, the eight calculations got averaged yielding the results for the correlators for one gauge configuration.

3.1.6. The Pseudoscalar Meson: The Pion

For the pseudoscalar meson one finds $\Gamma = \gamma_5$ (see Table 3.1):

$$O_{\pi^0}(n) = \frac{1}{\sqrt{2}}\left(\bar{u}(n)\gamma_5 u(n) - \bar{d}(n)\gamma_5 d(n)\right) \,. \tag{3.19}$$

The quantum numbers P and C are checked for the flavor-neutral interpolator for π^0 using the transformations discussed in Sect. 2.2.2, since the classification with C only strictly holds for flavor-neutral interpolators:

$$\begin{aligned} O_{\pi^0}(n) \xrightarrow{\mathcal{C}} O_{\pi^0}(n)^{\mathcal{C}} &= -\frac{1}{\sqrt{2}}\left(u(n)^T C\gamma_5 C^{-1}\bar{u}(n)^T - d(n)^T C\gamma_5 C^{-1}\bar{d}(n)^T\right) \\ &= \frac{1}{\sqrt{2}}\left(\bar{u}(n)\gamma_5 u(n) - \bar{d}(n)\gamma_5 d(n)\right)^T = O_{\pi^0}(n) \Rightarrow C = + \,, \end{aligned} \tag{3.20}$$

$$\begin{aligned} O_{\pi^0}(n) \xrightarrow{\mathcal{P}} O_{\pi^0}(n)^{\mathcal{P}} &= \frac{1}{\sqrt{2}}\left(\bar{u}(-\mathbf{n}, n_\tau)\gamma_4\gamma_5\gamma_4 u(-\mathbf{n}, n_\tau) - \bar{d}(-\mathbf{n}, n_\tau)\gamma_4\gamma_5\gamma_4 d(-\mathbf{n}, n_\tau)\right) \\ &= -\frac{1}{\sqrt{2}}\left(\bar{u}(-\mathbf{n}, n_\tau)\gamma_4^2\gamma_5 u(-\mathbf{n}, n_\tau) - \bar{d}(-\mathbf{n}, n_\tau)\gamma_4^2\gamma_5 d(-\mathbf{n}, n_\tau)\right) \\ &= -O_{\pi^0}(-\mathbf{n}, n_\tau) \Rightarrow P = - \,, \end{aligned} \tag{3.21}$$

where $u(n) \coloneqq \psi^{(u)}(n)$, $d(n) \coloneqq \psi^{(d)}(n)$, the relation for the charge conjugation matrix (2.34), and the anti-commutation relations for γ_5 (A.3) and for all γ_μ (A.2), which imply $\gamma_4^2 = \mathbb{1}_{4\times4}$, have been used. The interchange of the Grassmann variables during the transposition cancels a minus sign in the charge conjugation. Using exact isospin symmetry, i.e. two mass-degenerate quarks, and (3.8), the fermionic part of the expectation value of the correlator for the pseudoscalar meson, the pion, is for both, flavor-neutral and non-flavor-neutral pions,

$$\langle O_\pi(n)\bar{O}_\pi(m)\rangle_F = -\mathrm{tr}\left[(D^{-1}(n|m))^\dagger\gamma_5^2 D^{-1}(n|m)\gamma_5^2\right] . \tag{3.22}$$

With $\gamma_5^2 = \mathbb{1}$ (see (A.3)) and using point sources placed at $m = m_0 = 0$ one finds

$$\langle O_\pi(n)\bar{O}_\pi(0)\rangle_F = \sum_{\beta_0,b_0}\left(-\sum_{\alpha,a}|D^{-1}(n|0)^{\alpha\beta_0}_{ab_0}|^2\right) , \tag{3.23}$$

where the sum over the indices β_0, b_0 of the point sources is formally written before the sum over α, a because in CL^{2}QCD, the function called to calculate the correlator only takes one point source (which has the structure of a spinor) and calculates the sum over α, a, i.e. minus the spinor squarenorm. The summation over β_0, b_0 is done by calling this function 12 times, which is called a spin-color-wise computation in Sect. 5.2. This correlator can now be implemented and calculated for various simulation parameters using (3.16).

3.1.7. The Vector Meson: The ρ-Meson

For the vector meson one finds $\Gamma = \gamma_4\gamma_i, i = 1, 2, 3$ (see Table 3.1):

$$O_{\rho^0,i}(n) = \frac{1}{\sqrt{2}}\left(\bar{u}(n)\gamma_4\gamma_i u(n) - \bar{d}(n)\gamma_4\gamma_i d(n)\right) . \tag{3.24}$$

As for the pion, the quantum numbers P and C are checked for the flavor-neutral interpolator for ρ^0 using the transformations discussed in Sect. 2.2.2, since the classification with C only strictly holds for flavor-neutral interpolators:

$$\begin{aligned} O_{\rho^0,i}(n) \xrightarrow{\mathcal{C}} O_{\rho^0,i}(n)^{\mathcal{C}} &= -\frac{1}{\sqrt{2}}\left(u(n)^T(\gamma_i\gamma_4)^T\bar{u}(n)^T - d(n)^T(\gamma_i\gamma_4)^T\bar{d}(n)^T\right) \\ &= -O_{\rho^0,i}(n) \Rightarrow C = - , \end{aligned} \tag{3.25}$$

$$\begin{aligned} O_{\rho^0,i}(n) \xrightarrow{\mathcal{P}} O_{\rho^0,i}(n)^{\mathcal{P}} &= -\frac{1}{\sqrt{2}}\left(\bar{u}(-\mathbf{n},n_\tau)\gamma_4\gamma_i u(-\mathbf{n},n_\tau) - \bar{d}(-\mathbf{n},n_\tau)\gamma_4\gamma_i d(-\mathbf{n},n_\tau)\right) \\ &= -O_{\rho^0,i}(-\mathbf{n},n_\tau) \Rightarrow P = - , \end{aligned} \tag{3.26}$$

where the relation for the charge conjugation matrix (2.34) and the anti-commutation relations for all γ_μ (A.2), which imply $\gamma_4^2 = \mathbb{1}_{4\times4}$, have been used. The interchange of the Grassmann variables during the transposition cancels a minus sign in the charge conjugation. Again, using exact isospin symmetry and (3.8), the fermionic part of the expectation value of the correlator for the vector meson, the ρ-meson, is for flavor-neutral and non-flavor-neutral mesons

$$\langle O_{\rho,i}(n)\bar{O}_{\rho,i}(m)\rangle_F = -\mathrm{tr}\left[(D^{-1}(n|m))^\dagger\gamma_4\gamma_i\gamma_5 D^{-1}(n|m)\gamma_4\gamma_i\gamma_5\right] . \tag{3.27}$$

Point sources are again placed at $m = m_0 = 0$ and the propagator is given as $D^{-1}(n|0)_{\substack{\alpha\beta \\ c_1c_2}}$ for a point source $(0, \beta, c_2)$ in the following way, where $a, b, \ldots, q \in \mathbb{C}^{3\times3}$ are matrices in color space:

$$D^{-1}(n|0)_{\substack{\alpha\ \beta \\ c_1c_2}} = \begin{pmatrix} a & e & j & n \\ b & f & k & o \\ c & g & l & p \\ d & h & m & q \end{pmatrix} . \tag{3.28}$$

In the following, tr always indicates a trace over spin-color indices and tr_c always indicates a trace only over color indices. The fermionic part of the expectation value of the correlator in x-direction ($i = 1$) evaluates to

$$\begin{aligned} \langle O_{\rho,1}(n)\bar{O}_{\rho,1}(0)\rangle_F &= -\,\mathrm{tr}\left[(D^{-1}(n|0))^\dagger\gamma_4\gamma_1\gamma_5 D^{-1}(n|0)\gamma_4\gamma_1\gamma_5\right] \\ &= 2\ \mathrm{Re}\left(\mathrm{tr}_c\left[a^\dagger f + b^\dagger e + c^\dagger h + d^\dagger g + j^\dagger o + k^\dagger n + l^\dagger q + m^\dagger p\right]\right) \\ &= \sum_{c_2=1}^{3} 2 \sum_{c_1=1}^{3} \mathrm{Re}\,(a^*_{c_1c_2} f_{c_1c_2} + b^*_{c_1c_2} e_{c_1c_2} + c^*_{c_1c_2} h_{c_1c_2} + d^*_{c_1c_2} g_{c_1c_2} \\ &\qquad + j^*_{c_1c_2} o_{c_1c_2} + k^*_{c_1c_2} n_{c_1c_2} + l^*_{c_1c_2} q_{c_1c_2} + m^*_{c_1c_2} p_{c_1c_2})\ , \end{aligned} \tag{3.29}$$

Similarly, one finds in y- and z-direction ($i = 2, 3$):

$$\langle O_{\rho,2}(n)\bar{O}_{\rho,2}(0)\rangle_F = 2\ \mathrm{Re}\left(\mathrm{tr}_c\left[a^\dagger f - b^\dagger e + c^\dagger h - d^\dagger g + j^\dagger o - k^\dagger n + l^\dagger q - m^\dagger p\right]\right)\ , \tag{3.30}$$

$$\begin{aligned} \langle O_{\rho,3}(n)\bar{O}_{\rho,3}(0)\rangle_F = \mathrm{tr}_c\big[&a^\dagger a - b^\dagger b + c^\dagger c - d^\dagger d - e^\dagger e + f^\dagger f - g^\dagger g + h^\dagger h \\ &+ j^\dagger j - k^\dagger k + l^\dagger l - m^\dagger m - n^\dagger n + o^\dagger o - p^\dagger p + q^\dagger q\big]\ . \end{aligned} \tag{3.31}$$

As it can be seen from these correlators, the vector meson correlators can be evaluated for all three $c_2 = 1, 2, 3$ fixed and then, the results can be added to get the total correlators. This is called a color-wise computation in Sect. 5.2. The formulae for the vector meson correlator can now be implemented into a program and evaluated for different simulation parameters using (3.16).

3.2. The Effective Mass

This section deals with the relation between the correlators and the masses of the particles described by the correlators. All computations in this thesis are zero temperature calculations. Therefore, the zero temperature limit $N_\tau \to \infty$, while $aN_\tau \to \infty$ for the continuum limit $a \to 0$ (cf. Sect. 2.2.3), has to be taken in order for the equations in this section to be exact. It must then be verified in simulations that they took place at a sufficiently large N_τ such that the results are within the behavior explained here and one does not see temperature effects.

Starting with (2.40) and taking the zero temperature limit, the path integral expression for the correlator can be rewritten into the statistical mechanics expression (cf. (2.43))

$$\lim_{N_\tau\to\infty}\langle\tilde{O}(\mathbf{0}, n_\tau)\bar{O}(0)\rangle = Z^{-1}\mathrm{tr}\left[\mathrm{e}^{-(N_\tau-n_\tau)a\hat{H}}\hat{O}\ \mathrm{e}^{-n_\tau a\hat{H}}\hat{O}^\dagger\right]\ , \tag{3.32}$$

where now $\hat{O}$ and $\hat{O}^\dagger$ annihilate and create mesons with zero momentum and the euclidean time transporter was used to bring the operator $\hat{O}$ from time an_τ to 0. The correlator then becomes [cf. GL10, pp. 4-6], [cf. Phi10, p. 10],

$$\begin{aligned}\lim_{N_\tau\to\infty}\langle\tilde{O}(\mathbf{0},n_\tau)\bar{O}(0)\rangle &= \lim_{N_\tau\to\infty}\frac{\sum_{m,n}\langle m|\,\mathrm{e}^{-(N_\tau-n_\tau)a\hat{H}}\hat{O}\,|n\rangle\,\langle n|\,\mathrm{e}^{-n_\tau a\hat{H}}\hat{O}^\dagger\,|m\rangle}{Z}\\ &= \lim_{N_\tau\to\infty}\frac{\sum_{m,n}\langle m|\,\hat{O}\,|n\rangle\,\langle n|\,\hat{O}^\dagger\,|m\rangle\,\mathrm{e}^{-(N_\tau-n_\tau)aE_m}\mathrm{e}^{-n_\tau aE_n}}{\sum_n \mathrm{e}^{-aN_\tau E_n}}\\ &= \lim_{N_\tau\to\infty}\frac{\sum_{m,n}\langle m|\,\hat{O}\,|n\rangle\,\langle n|\,\hat{O}^\dagger\,|m\rangle\,\mathrm{e}^{-(N_\tau-n_\tau)a\Delta E_m}\mathrm{e}^{-n_\tau a\Delta E_n}}{1+\mathrm{e}^{-aN_\tau\Delta E_1}+\mathrm{e}^{-aN_\tau\Delta E_2}+\ldots}\,.\end{aligned}$$

$\Delta E_n \coloneqq E_n - E_0$ and E_0 is the vacuum energy. Since in the limit $N_\tau\to\infty$ also $aN_\tau\to\infty$ is implied, the denominator is equal to 1 and in the numerator only terms with $E_m = E_0$ survive, which holds only for the vacuum. With the identification $\Delta E_n \to E_n$ the final formula is

$$\lim_{N_\tau\to\infty}\langle\tilde{O}(\mathbf{0},n_\tau)\bar{O}(0)\rangle = \sum_n \left|\langle 0|\,\hat{O}\,|n\rangle\right|^2 \mathrm{e}^{-an_\tau E_n}\,. \tag{3.33}$$

The effective mass $am_{\mathrm{eff}} = am_{\mathrm{eff}}(n_\tau)$ (a for lattice units) is defined by [cf. GL10, p. 145]

$$\frac{\lim_{N_\tau\to\infty}\langle\tilde{O}(\mathbf{0},n_\tau)\bar{O}(0)\rangle}{\lim_{N_\tau\to\infty}\langle\tilde{O}(\mathbf{0},n_\tau+1)\bar{O}(0)\rangle} =: \mathrm{e}^{am_{\mathrm{eff}}(n_\tau)}\,. \tag{3.34}$$

For $n_\tau\to\infty$ (3.33) turns into

$$\lim_{N_\tau\to\infty}\langle\tilde{O}(\mathbf{0},n_\tau)\bar{O}(0)\rangle \xrightarrow{n_\tau\to\infty} \left|\langle 0|\,\hat{O}\,|1\rangle\right|^2 \mathrm{e}^{-an_\tau E_1}\,, \tag{3.35}$$

$|1\rangle$ is the lowest state with $\langle 0|\,\hat{O}\,|1\rangle \neq 0$, i.e. the ground state of the meson described by the correlator, and E_1 is its energy, which is equal to its mass m for zero momentum. Therefore, it is obvious that for $n_\tau\to\infty$, $am_{\mathrm{eff}}(n_\tau)$ becomes constant and $am = \lim_{n_\tau\to\infty} am_{\mathrm{eff}}(n_\tau)$.

For a periodic lattice, which is realized in all simulations in this thesis, mesons can not only propagate in n_τ, but also in $(N_\tau - n_\tau)$ [cf. GL10, pp. 144-145], thus propagating through the boundary. Hence, there is also a contribution from the second propagation resulting in a total behavior described by a shifted hyperbolic cosine. Eqs. (3.33) and (3.35) become

$$\lim_{N_\tau\to\infty}\langle\tilde{O}(\mathbf{0},n_\tau)\bar{O}(0)\rangle \xrightarrow{N_\tau\to\infty} \sum_n \left|\langle 0|\,\hat{O}\,|n\rangle\right|^2 \left(\mathrm{e}^{-an_\tau E_n} + \mathrm{e}^{-a(N_\tau-n_\tau)E_n}\right)\,. \tag{3.36}$$

The effective mass in this case is defined by [cf. GL10, p. 145]

$$\frac{\lim_{N_\tau\to\infty}\langle\tilde{O}(\mathbf{0},n_\tau)\bar{O}(0)\rangle}{\lim_{N_\tau\to\infty}\langle\tilde{O}(\mathbf{0},n_\tau+1)\bar{O}(0)\rangle} =: \frac{\mathrm{e}^{-n_\tau(am_{\mathrm{eff}}(n_\tau))} + \mathrm{e}^{-(N_\tau-n_\tau)(am_{\mathrm{eff}}(n_\tau))}}{\mathrm{e}^{-(n_\tau+1)(am_{\mathrm{eff}}(n_\tau))} + \mathrm{e}^{-(N_\tau-n_\tau-1)(am_{\mathrm{eff}}(n_\tau))}}\,. \tag{3.37}$$

For $n_\tau\to\infty$ (3.36) turns into

$$\langle\tilde{O}(\mathbf{0},n_\tau)\bar{O}(0)\rangle \xrightarrow{N_\tau,n_\tau\to\infty} \left|\langle 0|\,\hat{O}\,|1\rangle\right|^2 \left(\mathrm{e}^{-an_\tau E_1} + \mathrm{e}^{-a(N_\tau-n_\tau)E_1}\right)\,, \tag{3.38}$$

where terms like $\mathrm{e}^{-a(N_\tau-n_\tau)E_n}$ have been added to the original exponential terms to account for the mesons propagating in negative temporal direction. Note that the notation

for the limit $N_\tau \to \infty$ has been changed to account for the appearance of N_τ in the right-hand side of the equations. Therefore, the asymptotic behavior of the equations is meant. Again, it is obvious that for $n_\tau \to \infty$ (while still having $n_\tau \ll N_\tau$), $am_{\text{eff}}(n_\tau)$ becomes constant and $am = \lim_{n_\tau \to \infty} am_{\text{eff}}(n_\tau)$.

The effective meson mass can now be determined in a simulation (in lattice units) using a fit in the range where $am_{\text{eff}}(n_\tau)$ hits a plateau. Here one can assume that $0 \ll n_\tau \ll N_\tau$ such that $am \approx am_{\text{eff}}(n_\tau)$.

3.3. The PCAC Quark Mass

In this section, the fermionic part of the PCAC correlator, which is needed to determine the PCAC quark mass and to be able to do a chiral extrapolation in it, will be calculated. Since this section works explicitly with u- and d-quarks, the notation $\psi^{(u)} = u$ and $\psi^{(d)} = d$ will be used. As stated in Sect. 2.3, the PCAC relation with the axial ward identity can be used to calculate the PCAC quark mass on the lattice. For this, the pseudoscalar interpolator (2.69) and the axial vector field (2.70) first have to be transformed into creation and annihilation operators. Because τ^a are the Pauli matrices (A.7) and $\psi = (u, d)^T$, one can use the definitions

$$\tau^+ = \frac{1}{2}(\tau^1 + i\tau^2) = \begin{pmatrix} 0 & 1 \\ 0 & 0 \end{pmatrix} , \tag{3.39}$$

$$\tau^- = \frac{1}{2}(\tau^1 - i\tau^2) = \begin{pmatrix} 0 & 0 \\ 1 & 0 \end{pmatrix} , \tag{3.40}$$

to find that

$$\tau^+ \psi = (d, 0)^T, \tag{3.41}$$

$$\tau^- \psi = (0, u)^T. \tag{3.42}$$

Therefore, one finds using (2.69) and (2.70) [see GL10, p. 268]

$$P^+(n) = P^1(n) - iP^2(n) = (\bar{u}(n), \bar{d}(n))\gamma_5\tau^-(u(n), d(n))^T = \bar{d}(n)\gamma_5 u(n) , \tag{3.43}$$

$$P^-(n) = P^1(n) + iP^2(n) = (\bar{u}(n), \bar{d}(n))\gamma_5\tau^+(u(n), d(n))^T = \bar{u}(n)\gamma_5 d(n) , \tag{3.44}$$

$$A^+_\mu(n) = A^1_\mu(n) - iA^2_\mu(n) = (\bar{u}(n), \bar{d}(n))\gamma_\mu\gamma_5\tau^-(u(n), d(n))^T = \bar{d}(n)\gamma_\mu\gamma_5 u(n) , \tag{3.45}$$

$$A^-_\mu(n) = A^1_\mu(n) + iA^2_\mu(n) = (\bar{u}(n), \bar{d}(n))\gamma_\mu\gamma_5\tau^+(u(n), d(n))^T = \bar{u}(n)\gamma_\mu\gamma_5 d(n) . \tag{3.46}$$

The index on the interpolators refers to the electrical charge of the mesons that are annihilated by these operators. With Table 3.1 and eqs. (3.2) and (3.4) it is obvious that these operators are meson interpolators annihilating a pion $\pi^\pm$ and an axial vector meson with charge $\pm e$, and creating the meson with the other charge, just that the index for the axial vector interpolator here runs from 1 to 4.

Since the multiplicative renormalization connecting A^a_μ and $A^{(r)a}_\mu$ is not important for this calculation and a chiral extrapolation in the PCAC quark mass m_{PCAC}, (2.72) can be used with the meson interpolators from above to find that

$$\begin{aligned} \partial_\mu A^-_\mu(n) &= \partial_\mu A^1_\mu(n) + i\partial_\mu A^2_\mu(n) \\ &= 2m_{\text{PCAC}}(P^1(n) + iP^2(n)) = 2m_{\text{PCAC}}P^-(n) , \end{aligned} \tag{3.47}$$

$$\langle(\partial_\mu A^-_\mu(n))P^+(m)\rangle = 2m_{\text{PCAC}}\langle P^-(n)P^+(m)\rangle = 2m_{\text{PCAC}}\langle O_\pi(n)\bar{O}_\pi(m)\rangle . \tag{3.48}$$

The fact that $P^{\pm}$ are O_π and $\bar{O}_\pi$ has been used in the last step to clarify the connection. Note that all equations have been put on the lattice, which implies a discretized derivative. In order for these equations to make sense, $m_u = m_d$ has to be implied. Now, the source gets fixed at the origin $m = 0$ as before and with this, the derivative can be pulled out of the expectation value on the left-hand side of (3.48), which gives

$$\partial_\mu \langle A_\mu^-(n) P^+(0)\rangle = 2 m_{\mathrm{PCAC}} \langle P^-(n) P^+(0)\rangle \ . \tag{3.49}$$

The derivative only acts on $A_\mu(n)$ because the source is fixed at $m = 0$. Projecting to zero momentum using (3.15) leads to

$$\begin{aligned}
\partial_\mu \langle \tilde{A}_\mu^-(\mathbf{0}, n_\tau) P^+(0)\rangle &= \frac{1}{N_\sigma^3} \sum_{n_1,n_2,n_3} \partial_\mu \langle A_\mu^-(\mathbf{n}, n_\tau) P^+(0)\rangle \\
&= \frac{1}{N_\sigma^3} \sum_{n_1,n_2,n_3} \partial_4 \langle A_4^-(\mathbf{n}, n_\tau) P^+(0)\rangle \\
&= 2 m_{\mathrm{PCAC}} \langle \tilde{P}^-(\mathbf{0}, n_\tau) P^+(0)\rangle \qquad (3.50) \\
\Rightarrow m_{\mathrm{PCAC}} &= \frac{\partial_4 \langle \tilde{A}_4^-(\mathbf{0}, n_\tau) P^+(0)\rangle}{2\langle \tilde{P}^-(\mathbf{0}, n_\tau) P^+(0)\rangle} \ . \qquad (3.51)
\end{aligned}$$

The fact that all spatial derivatives give a vanishing contribution because of the sum and the periodic boundary conditions in all spatial directions has been used in the second line. (3.51) is often used as the definition for the PCAC quark mass [cf. Pin14, p. 19]. With the symmetrically discretized derivative (2.12), the PCAC quark mass in lattice units becomes

$$a m_{\mathrm{PCAC}} = \frac{1}{4} \frac{\langle \tilde{A}_4^-(\mathbf{0}, n_\tau + 1) P^+(0)\rangle - \langle \tilde{A}_4^-(\mathbf{0}, n_\tau - 1) P^+(0)\rangle}{\langle \tilde{P}^-(\mathbf{0}, n_\tau) P^+(0)\rangle} \ . \tag{3.52}$$

Note that the expression on the right-hand side still depends explicitly on n_τ, since (3.51) and (3.52) are only valid for $N_\tau, n_\tau \to \infty$ as for the effective mass. Besides, (3.52) differs from the corresponding formula in the paper used as a reference for the calculation of the critical hopping parameter $\kappa_c(\beta)$ [Iwa+96]. The difference can be explained by the factor of m_π in the formula in [Iwa+96], which comes from carrying out the derivative using a hyperbolic sine as an ansatz for the so-called AP-correlator.

In order to be able to implement the calculation of $a m_{\mathrm{PCAC}}$, the fermionic part of the correlator with the axial vector interpolator in n_τ-direction and the pseudoscalar interpolator has to implemented, also referred to by the AP-correlator. Using (3.43) - (3.46) and the same procedure as in Sect. 3.1, one finds

$$\begin{aligned}
\langle A_0^-(n) P^+(0)\rangle_F &= \langle \bar{u}(n)\gamma_4\gamma_5 d(n) \bar{d}(0)\gamma_5 u(0)\rangle_F \\
&= -(\gamma_4\gamma_5)_{\alpha_1\beta_1}(\gamma_5)_{\alpha_2\beta_2} \langle \bar{u}(n)_{\alpha_1 c_1} u(0)_{\substack{\beta_2 \\ c_2}}\rangle_u \langle \bar{d}(0)_{\substack{\alpha_2 \\ c_2}} d(n)_{\substack{\beta_1 \\ c_1}}\rangle_d \\
&= -\mathrm{tr}\left[\gamma_5 D^{-1}(0|n)\gamma_4\gamma_5 D^{-1}(n|0)\right] \ . \qquad (3.53)
\end{aligned}$$

The minus sign again comes from the reordering of the Grassmann variables and Wick's theorem (2.58) has been used in the third line. Using γ_5-hermicity (2.39) and $\{\gamma_\mu, \gamma_5\} = 0$, the correlator becomes

$$\langle A_0^-(n) P^+(0)\rangle_F = \mathrm{tr}\left[(D^{-1}(n|0))^\dagger \gamma_4 D^{-1}(n|0)\right] \ . \tag{3.54}$$

With (3.28) and using point sources placed at 0, the explicit form of the correlator is

$$\langle A_0^-(n) P^+(0)\rangle_F = -2\ \mathrm{Re}\left(\mathrm{tr}_c\left[a^\dagger c + b^\dagger d + e^\dagger g + f^\dagger h + j^\dagger l + k^\dagger m + n^\dagger p + o^\dagger q\right]\right) \ . \tag{3.55}$$

Note that since no columns of the quark propagator are mixed, the correlator can in fact be calculated spin-color-wise. Besides, the minus sign depends on the convention of the Dirac matrices. Knowing that am_{PCAC} is positive, one can simply take the absolute value when calculating (3.52).

4. Numerical Methods

After the fermionic part of the expectation values for the correlators was calculated in the last chapter, the first part of this chapter will detail the numerical methods, i.e. the hybrid Monte Carlo algorithm, to calculate the gauge part of the expectation values. In the second part of this chapter, the statistical method needed for analyzing the results of the hybrid Monte Carlo algorithm and the methods for the extraction of masses from the correlators will be introduced.

4.1. The Hybrid Monte Carlo Algorithm

In order to calculate the full expectation value for the correlators, one also has to calculate the gauge part as in (2.51), an integral over all possible gauge field configurations. Even for small lattice sizes, it can consist of thousands or even millions of integration variables and it usually cannot be done analytically. Because of the high dimensionality of the integral, one can only use importance sampling methods to estimate the integral. This is generally realized with a Monte Carlo (MC) algorithm, which creates a so-called Markov chain consisting of a set U_n of N gauge configurations distributed in the phase space of all gauge configurations according to the probability measure

$$\frac{1}{Z}\mathrm{e}^{-S_G[U]}\det[D]^2 \,, \tag{4.1}$$

where (2.60) has been plugged in for $Z_F[U]$. The estimate for the gauge part of the expectation value for an observable B as in (2.51) then becomes [cf. GL10, p. 73]

$$\langle B\rangle_G \approx \frac{1}{N}\sum_n B[U_n] \,. \tag{4.2}$$

For $N \to \infty$ (4.2) becomes exact. The relative error of the result of such an algorithm (i.e. an observable computed using a Monte Carlo simulation) is roughly $\propto 1/\sqrt{N}$ [see GL10, pp. 93-94].

One way to include the fermion determinant in the probability measure and therefore have dynamical fermions is the hybrid Monte Carlo (HMC) algorithm. As stated in Sect. 3.1.5, the Dirac operator has $\mathcal{O}(10^{12})$ entries. This makes a direct evaluation of $\det[D]$ impossible because it would need $\mathcal{O}((10^{12})!)$ operations. In the HMC algorithm, the action gets therefore rewritten into [see GL10, pp. 187-199]

$$S_{\text{eff}}[U,\phi,\phi^\dagger] = S_G[U] + \phi^\dagger(DD^\dagger)^{-1}[U]\phi \tag{4.3}$$

such that the probability distribution becomes

$$\frac{1}{Z}e^{-S_G[U]}\det[D]^2 = e^{-S_{\text{eff}}[U,\phi,\phi^\dagger]} \,, \tag{4.4}$$

where ϕ and $\phi^\dagger$ are so-called pseudofermion fields, which are bosonic fields. They are related to the fermion determinant via [cf. GL10, pp. 187-188], [cf. Pin14, pp. 29-30]

$$\det[D]^2 = \det[DD^\dagger] \propto \int \mathcal{D}[\phi]\mathcal{D}[\phi^\dagger]\ \mathrm{e}^{-\phi^\dagger(DD^\dagger)^{-1}\phi} \,. \tag{4.5}$$

The cyclicity of the trace and γ_5-hermicity (2.38) have been used to find [see GL10, p. 187]

$$\det[D]^* = \det[D^\dagger] = \det[\gamma_5 D \gamma_5] = \det[D] \tag{4.6}$$

$$\Rightarrow 0 \leq \det[D]^2 = \det[D]\det[D^\dagger] = \det[DD^\dagger] \; . \tag{4.7}$$

The second equation also ensures that (4.1) is real and non-negative for two mass-degenerate quark flavors and can thus be interpreted as a probability measure. In fact, this holds for any even number of mass-degenerate quark flavors [see GL10, p. 187].

One then constructs a fictitious classical molecular dynamics system with a Hamiltonian $H = \frac{1}{2}P^2 + S_{\text{eff}}$, where P are the conjugate momenta to U and elements of $\mathfrak{su}(3)$ consisting of 8 real-valued entries (for 3 colors, otherwise $\mathfrak{su}(N_c)$ with $(N_c \times N_c - 1)$ entries) for each lattice position and direction $P = P_\mu(n)$ [see Pin14, p. 31]. In the first step of the HMC algorithm, P and ϕ are generated with the distributions $\exp(-(D^{-1}\phi)^\dagger D^{-1}\phi)$ and $\exp(-\frac{1}{2}P^2)$ respectively. A given configuration (U, P) then gets evolved to a new configuration (U', P') over a time τ according to the Hamilton's equations of motion [see Pin14, p. 31]

$$\dot{P} = -\frac{\partial S_{\text{eff}}}{\partial U} \equiv F \; , \tag{4.8}$$

$$\dot{U} = P \tag{4.9}$$

using the leapfrog or the second order minimal integration scheme [Td06]. $F = F_G + F_F$ is the force term and has contributions from gauge and from fermion terms [cf. Pin14, p. 31]. One can control the accuracy of the integration with the number of integration steps I and, therefore, a minimal step size $\Delta\tau = \tau / I$. At the end of each evolution step, one accepts the new configuration with a probability

$$P_{\text{acc}} = \min(1, \exp(H[P', U'] - H[P, U])) \; . \tag{4.10}$$

In order to improve the algorithm, one typically chooses a different number of integration steps for the gauge and fermionic contributions to the force, i.e. more steps for the gauge part, which is numerically cheaper to calculate, a technique called multiple timescales [Urb+06]. Since the inversion of the Dirac operator, which has to be used in order to calculate $\det[D]$, gets more expensive with decreasing quark mass, one can use mass preconditioning [Has01], which uses $\det[D] = \frac{\det[D]}{\det[A]}\det[A]$, thus introducing a new Dirac operator A with a higher quark mass, i.e. a lower $\kappa = \kappa_{\text{mp}}$ than the κ for D, which is therefore cheaper to invert. Using multiple timescales for the different fermions leads to a less expensive integration.

The inversion of the Dirac operator is done using a Krylov solver, usually either with the Conjugate Gradient (CG) algorithm, which in its original version only works for positive definite symmetric matrices, or the Bi-conjugate Gradient Stabilized (Bi-CGStab) algorithm, which works on any matrix, but may not always converge. For further information see [GL10, pp. 138-141], [Pin14, pp. 32-33].

This short introduction to HMC has been oriented by [Pin14, pp. 29-30]. For more details see also [GL10, pp. 185-199].

4.1.1. Generation of Gauge Configurations

In order to create gauge configurations, which in the case of CL^{2}QCD is done using the executable `hmc`, one first needs to initialize the link variables either all to $\mathbb{1}_{3\times3}$ (cold start)

or to random matrices in color space (hot start). Then, the HMC algorithm gets started. At the beginning of a simulation, the configurations generated, i.e. the Markov chain, do not follow the equilibrium distribution (4.1). Therefore, one has to perform usually around one thousand steps until one can start evaluating the observables, which is also often referred to by measuring the observables. A good estimate to when the system of the link variables is in equilibrium is the expectation value of the plaquette. The procedure of reaching the equilibrium distribution is called thermalization.

Since the acceptance rate P_{app} depends on the number of integration steps for the different contributions to the force and also on whether or not mass preconditioning is applied, it has to be tuned for the HMC algorithm to give good results. In the context of this thesis, it is tuned so that $70\% \lesssim P_{\text{acc}} \lesssim 80\%$. The tuning can be done at the end of the thermalization, when the Markov chain is already almost in equilibrium.

After thermalization and tuning, the configurations for evaluating the observables can be produced. Usually, one uses different seeds of the pseudo random number generator (PRNG) needed in several steps of the HMC algorithm to be able to start multiple different HMC chains running in parallel on different CPUs or graphical processing units (GPUs) to decrease the total simulation time, i.e. to produce multiple different Markov chains at the same time.

One does not evaluate the observables on all configurations that are visited by the HMC algorithm, since the step from one configuration to another is too small to ensure uncorrelated configurations. Thus, using all configurations would result in a high autocorrelation and an error that may be underestimated (see Sect. 4.2 for more details). For this thesis, it turned out that evaluating the observables, i.e. the correlators discussed in Sect. 3, for every 50th configuration gives acceptable autocorrelation times.

After sufficiently many gauge configurations for measurement have been generated, one can evaluate the observables of interest. The results of these evaluations are then analyzed using statistical methods discussed in Sect. 4.2. Afterwards, one has to check that the error as well as the autocorrelation time is small enough. If not, more simulations have to be performed.

4.2. Statistical Analysis and Fits

4.2.1. The Γ-Method

The Γ-method (ΓM) by Ulli Wolff is a method for the statistical analysis of the results of Monte Carlo simulations allowing more exact error estimates than binning techniques, especially with regard to autocorrelation. To do so, it calculates an estimate of the autocorrelation function. A detailed description of the original method can be found in [Wol04]. There is also an improved version with a τ_{exp} bias correction presented in [SSV11][1], but even though this program has been used as it is being used in the working group, the correction has not been used in the context of this thesis.

[1] This is the given citation with the proposal for the improvement. For the code with a description see `http://www-zeuthen.desy.de/alpha/public_software/UWerrTexp.html`

The objective of the Γ-method is to calculate a function f of primary observables with exact statistical mean values A_α [see Wol04, p. 2]

$$F \equiv f(A_1, A_2, \ldots) \equiv f(A_\alpha) \ . \tag{4.11}$$

In order to estimate the function, A_α gets estimated using a (H)MC algorithm by $a_\alpha^{i,r}$, where $i = 1, 2, \ldots, N_r$ is the number of the Monte Carlo configuration in each Markov chain and $r = 1, 2, \ldots, R$ refers to the number of statistically independent replica [see Wol04, p. 3], for example from running multiple HMC chains in parallel as described in Sect. 4.1.2. The autocorrelation function is then defined by [see Wol04, p. 3]

$$\langle (a_\alpha^{i,r} - A_\alpha)(a_\beta^{j,s} - A_\beta) \rangle =: \delta_{rs} \Gamma_{\alpha\beta}(j - i) \tag{4.12}$$

and only depends on the distance in time in the Markov chain $j - i$. The notation $\langle \cdot \rangle$ in this discussion of the ΓM is used to refer to an "ensemble of identical numerical experiments with independent random numbers and initial states" [see Wol04, p. 3].

The per replicum mean is defined as

$$\bar{a}_\alpha^r = \frac{1}{N_r} \sum_{i=1}^{N_r} a_\alpha^{i,r} \tag{4.13}$$

such that

$$\bar{\bar{a}}_\alpha = \frac{1}{N} \sum_{r=1}^{R} N_r \bar{a}_\alpha^r \tag{4.14}$$

is the estimator of A_α [see Wol04, p. 4]. The estimator for F is given by [see Wol04, p. 5]

$$\bar{\bar{F}} = f(\bar{\bar{a}}_\alpha) \ . \tag{4.15}$$

Using

$$C_{\alpha\beta} = \sum_{t=-\infty}^{\infty} \Gamma_{\alpha\beta}(t) \tag{4.16}$$

the covariance matrix for F is

$$C_F = \sum_{\alpha\beta} f_\alpha f_\beta C_{\alpha\beta} \ , \tag{4.17}$$

where

$$f_\alpha = \frac{\partial f}{\partial A_\alpha} \ . \tag{4.18}$$

The error is given by

$$\sigma_F^2 = \frac{2\tau_{\mathrm{int},F}}{N} v_F = \frac{C_F}{N} \ . \tag{4.19}$$

There,

$$v_F = \sum_{\alpha,\beta} f_\alpha f_\beta \Gamma_{\alpha\beta}(0) \tag{4.20}$$

is the effective 'naive' variance relevant for F and

$$\tau_{\mathrm{int},F} = \frac{1}{2v_F} \sum_{t=-\infty}^{\infty} \sum_{\alpha,\beta} f_\alpha f_\beta \Gamma_{\alpha\beta}(t) \tag{4.21}$$

is the integrated autocorrelation time for F [see Wol04, p. 6]. As stated also there, for no autocorrelations $2\tau_{\mathrm{int},F} = 1$ (4.19) is the standard error and for a purely exponential

behavior, $\Gamma_{\alpha\beta}(t) \propto \exp(-|t|/\tau)$, the autocorrelation time τ is related to the integrated one by $\tau_{\mathrm{int},F} = \tau + \mathcal{O}(\tau^{-1})$. Besides, only $N/(2\tau_{\mathrm{int},F})$ of the estimates contribute to a smaller statistical error [see Wol04, p. 6].

The ΓM estimates the autocorrelation function for the primary observables a_α and for F by [see Wol04, pp. 7-9]

$$\bar{\bar{\Gamma}}_{\alpha\beta}(t) = \frac{1}{N - Rt} \sum_{r=1}^{R} \sum_{i=1}^{N_r - t} (a_\alpha^{i,r} - \bar{\bar{a}}_\alpha)(a_\beta^{i+t,r} - \bar{\bar{a}}_\beta) \;, \tag{4.22}$$

$$\bar{\bar{\Gamma}}_F(t) = \sum_{\alpha,\beta} \bar{\bar{f}}_\alpha \bar{\bar{f}}_\beta \bar{\bar{\Gamma}}_{\alpha\beta}(t) \;, \tag{4.23}$$

where

$$\bar{\bar{f}}_\alpha \approx \frac{1}{2h_\alpha}(f(\bar{\bar{a}}_1, \bar{\bar{a}}_2, \ldots, \bar{\bar{a}}_\alpha + h_\alpha, \ldots) - f(\bar{\bar{a}}_1, \bar{\bar{a}}_2, \ldots, \bar{\bar{a}}_\alpha - h_\alpha, \ldots)) \;, \tag{4.24}$$

$$h_\alpha = \sqrt{\frac{\bar{\bar{\Gamma}}_{\alpha\alpha}(0)}{N}} \;, \tag{4.25}$$

such that the estimators for v_F and C_F become

$$\bar{\bar{v}}_F = \bar{\bar{\Gamma}}_F(0) \;, \tag{4.26}$$

$$\bar{\bar{C}}_F(W) = \left[\bar{\bar{\Gamma}}_F(0) + 2\sum_{t=1}^{W} \bar{\bar{\Gamma}}_F(t)\right] \;. \tag{4.27}$$

W has to be chosen such that the total (i.e. the sum of the statistical and the systematic error) relative error of the estimate of the error $\bar{\bar{\sigma}}_F$

$$\frac{\delta_{\mathrm{tot}}(\bar{\bar{\sigma}}_F)}{\bar{\bar{\sigma}}_F} \approx \frac{1}{2} \min_W \left(\exp(-W/\tau) + 2\sqrt{W/N}\right) \tag{4.28}$$

is minimized. The error estimate then is

$$\bar{\bar{\sigma}}_F^2 = \frac{\bar{\bar{C}}_F(W)}{N} \;, \tag{4.29}$$

which is evaluated at optimal W. Denoting errors of quantities with $\delta(\cdot)$ and using [see Wol04, p. 9]

$$\delta(\bar{\bar{C}}_F) = \langle(\bar{\bar{C}}_F(W) - C_F)^2\rangle \approx \frac{2(2W+1)}{N} C_F^2 \tag{4.30}$$

together with error propagation from (4.19) and (4.29), one finds

$$\delta(\bar{\bar{\sigma}}_F) = \frac{1}{2\sqrt{C_F N}} \delta(\bar{\bar{C}}_F) \approx \sqrt{\frac{W + \frac{1}{2}}{N}}\; \sigma_F \approx \sqrt{\frac{W + \frac{1}{2}}{N}}\; \bar{\bar{\sigma}}_F \;. \tag{4.31}$$

The exact quantities have been used at the beginning of the calculation and have been replaced by the estimated quantities at the end in order to give an estimate of the error of the error.

The estimate of the integrated autocorrelation time and its error are [see Wol04, p. 10]

$$\bar{\bar{\tau}}_{\mathrm{int},F} = \frac{\bar{\bar{C}}_F(W)}{2\bar{\bar{v}}_F} \,, \tag{4.32}$$

$$\delta(\bar{\bar{\tau}}_{\mathrm{int},F}) \approx 2\bar{\bar{\tau}}_{\mathrm{int},F}\sqrt{\frac{(W+\frac{1}{2}-\bar{\bar{\tau}}_{\mathrm{int},F})}{N}} \,, \tag{4.33}$$

where, in contrast to the corresponding eq. (42) in [Wol04, p. 10], in the last expression the estimate $\tau_{\mathrm{int},F}$ has been plugged in on the right-hand side in order to be able to give an estimate. Each expression is to be evaluated at the optimal W from above.

The ΓM is available for `Matlab` without [Wol04][2] and with the τ_{exp} bias correction [SSV11][3]. A standard call is [see Wol04, pp. 17-19]

```
[value,dvalue,ddvalue,tauint,dtauint,Q] = ...
UWerr(Data,Stau,Nrep,Name,Quantity,P1,P2,...)
```

`Data` is a matrix with the rows being $a_\alpha^{i,r}$ for i, r fixed and all values of α, `Stau` is a value needed for the algorithm of finding W and can in the context of this thesis just be left at its default value 1.5, `Nrep` $= [N_1, N_2, \ldots, N_r]$, `Name` is the name in the title for the generated plots, `Quantity` is the reference `@fun` of a function `fun`, which resembles $f(A_\alpha)$ from (4.11), and `P1,P2,...` are optional additional parameters for `fun`. `value` is the estimate of F according to (4.15), `dvalue` is the estimate of σ_F according to (4.29), `ddvalue` is the estimate of $\delta(\bar{\bar{\sigma}}_F)$ according to (4.31), `tauint` is the estimate of $\tau_{\mathrm{int},F}$ according to (4.32), `dtauint` is the estimate of $\delta(\bar{\bar{\tau}}_{\mathrm{int},F})$, and `Q` describes how well the per-replicum estimates $f(\bar{a}_\alpha^r)$, where only r is fixed, are agreeing with each other [see Wol04, p. 7].

As stated before, the function used is in fact a modified version of the ΓM with τ_{exp} bias correction, but it is called in a way such that it only performs the standard analysis described here.

4.2.2. Fits

The standard method for fitting a set of data points $\{(x_i, y_i, \sigma_i)\}$, where σ_i is the error on the y_i values corresponding to x_i and $i = 1, 2, \ldots, N$, to a fitting function $f(x)$ is by minimizing [see You12, p. 20]

$$\chi^2 = \sum_{i=1}^{N} \left(\frac{y_i - f(x_i)}{\sigma_i} \right)^2 \,. \tag{4.34}$$

The value of χ^2/N_{DOF}, where N_{DOF} is the number of degrees of freedom in the fit, gives a first idea of whether a fit is good or not. Since a fit minimizes χ^2, a high value of $\chi^2/N_{\mathrm{DOF}} \gg 1$ indicates that the data points are not on the fitted function within their errors. When $\chi^2/N_{\mathrm{DOF}} \ll 1$, there might be some over-fitting, i.e. there are too many fit parameters and the data is over-described. However, this is not the case in this thesis, since e.g. the data produced for the effective and PCAC quark masses is often very good. Ideal is a value of $\chi^2/N_{\mathrm{DOF}} \approx 1$.

[2] `https://www.physik.hu-berlin.de/de/com/ALPHAsoft`
[3] `http://www-zeuthen.desy.de/alpha/public_software/UWerrTexp.html`

Another important quantity to measure the goodness of a fit is denoted by Q and given by [see You12, p. 26]

$$Q = \frac{1}{\Gamma(N_{\mathrm{DOF}}/2)} \int_{\chi^2/2}^{\infty} y^{(N_{\mathrm{DOF}}/2)-1} \mathrm{e}^{-y} dy \ , \tag{4.35}$$

where $\Gamma(x)$ is the Euler gamma function [see You12, p. 59]. $0 \leq Q \leq 1$ gives the probability that "given the fit, the data could have occured with a χ^2 greater than or equal to the value found" when assuming Gaussian noise on the data [see You12, p. 26]. A value of $Q \approx 0.5$ is considered to be optimal.

Fitting procedures give an error estimate of the fit parameters. Details on how this is done using the covariance matrix are given in [You12, pp. 23-29]. One important thing to keep in mind when using `gnuplot`[4] as in this thesis is that it gives out the asymptotic standard error instead of the proper error on the fit parameters [see You12, p. 62]. Therefore, one has to divide the asymptotic standard errors given out by `gnuplot` by what it calls `FIT_STDFIT`, which is equal to $\sqrt{\chi^2/N_{\mathrm{DOF}}}$ [see You12, p. 62].

4.2.3. The Effective Mass from the Γ-Method

First, define $C(n_\tau) \coloneqq \lim_{N_\tau \to \infty} \langle \tilde{O}(\mathbf{0}, n_\tau) O(0) \rangle$ and recall that the limit is realized in all simulations by having $N_\tau \approx 2N_\sigma$. Then, the first step in extracting a meson mass from a meson correlator is applying periodicity (cf. (3.38)) to find that $C(n_\tau) = C(N_\tau - n_\tau)$. Let N_τ be even, which is true for all simulations in this thesis. Thus, one sets $(C(n_\tau) + C(N_\tau - n_\tau))/2, 0 < n_\tau < N_\tau/2$ as $C(n_\tau)$ to average out fluctuations. $C(0)$ and $C(N_\tau/2)$ are not replaced because there is no correlator position with which they can be averaged. This is done for every result for the correlators given out by the executable `inverter` using the gauge configurations from the HMC algorithm. To ensure that all correlators are positive, since possible sign changes have been neglected in the calculation and they are supposed to be strictly positive according to (3.33) and (3.36), $C(n_\tau)$ is replaced by $|C(n_\tau)|$ for all $0 \leq n_\tau \leq N_\tau/2$.

With $x \coloneqq \mathrm{e}^{am_{\mathrm{eff}}(n_\tau)} > 1,\ 0 \leq n_\tau \leq N_\tau - 1$, since $am_{\mathrm{eff}}(n_\tau) > 0$, (3.37) becomes

$$\begin{aligned} r \coloneqq \frac{C(n_\tau)}{C(n_\tau + 1)} &= \frac{x^{-n_\tau} + x^{-(N_\tau - n_\tau)}}{x^{-n_\tau - 1} + x^{-(N_\tau - n_\tau - 1)}} \\ &= \frac{x^{\tau} + x^{-\tau}}{x^{\tau - 1} + x^{-\tau + 1}} \ , \end{aligned} \tag{4.36}$$

where $\tau = N_\tau/2 - n_\tau$. Rewriting gives

$$f(x) \coloneqq r(x^{\tau-1} + x^{-\tau+1}) - (x^{\tau} + x^{-\tau}) = 0 \ , \tag{4.37}$$

which means that finding $am_{\mathrm{eff}}(n_\tau)$ corresponds to finding the absolute zero of $f(x)$, where $x > 0$. This can be done using Newton's method [see BS80, pp. 782-783], which converges quadratically, i.e. it doubles the number of significant figures every iteration. With

$$f'(x) = r\tau(x^{\tau-2} - x^{-\tau}) - \tau(x^{\tau-1} - x^{-\tau-1}) \tag{4.38}$$

and by setting $x_0 = r$, i.e. the value for a purely exponential behavior, cf. (3.34), one can iterate

$$x_{m+1} = x_m - \frac{f(x_m)}{f'(x_m)} \tag{4.39}$$

[4] `http://www.gnuplot.info`

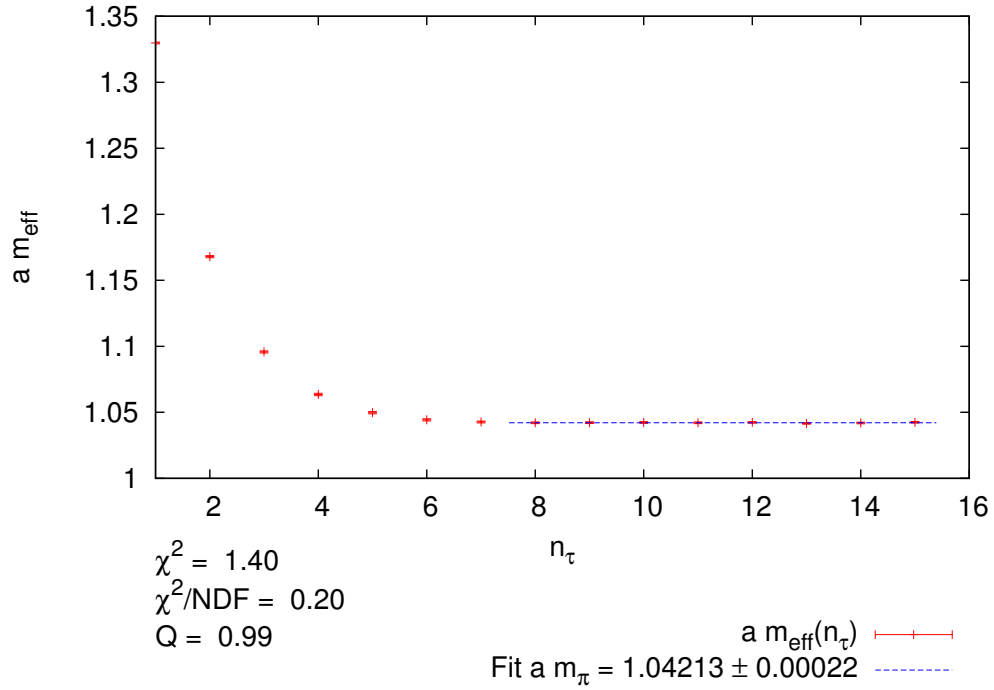

Figure 4.1.: Effective mass plot and fit for pion at $(\beta, \kappa) = (5.2420, 0.1650)$.

to find x with good precision. In the context of this thesis there have been two ways implemented for the iteration to stop. Either when $|f(x_m)| < 10^{-15}$ or when $|x_{m+1} - x_m| < 10^{-10}$, thus ensuring that the iteration will stop at a precision better than the accuracy of the HMC algorithm. Since $f(x) = f(1/x)$, there are two x, where $f(x) = 0$. In order to be sure that the effective mass is positive, $am_{\text{eff}}(n_\tau) = |\ln(x)| \geq 0$ is set, where x is the result of Newton's method. This method of finding $am_{\text{eff}}(n_\tau)$ has been programmed in `Matlab` in the course of this thesis. It can be passed as the argument for `fun` to the ΓM, so that $am_{\text{eff}}(n_\tau)$ is computed for every $0 \leq n_\tau < N_\tau/2$ using the ΓM and the pre-averaged correlators from the HMC calculation.

After $am_{\text{eff}}(n_\tau)$ has been calculated it gets plotted against n_τ and fitted to a constant in the region, where it is constant within its errors, using `gnuplot`. The goodness of the fit has to be evaluated using χ^2/N_{DOF} and Q, thus validating that the limit $n_\tau \to \infty$ is approximately fulfilled and the fit to a constant is valid. It might be appropriate to exclude values of $am_{\text{eff}}(n_\tau)$ at high $n_\tau \approx N_\tau/2$ from the fit because of large errors that can occur in this region. The fit gives the mass am of the meson in lattice units with its (corrected) error. An example plot and fit for the pion mass at $(\beta, \kappa) = (5.2420, 0.1650)$ generated in the course of this thesis can be found in Fig. 4.1. In this plot one can see that the effective mass hits a plateau at a distance of $n_\tau = 8$ from the source to the sink keeping in mind the periodic boundaries. Therefore, a fit has been performed from $n_\tau = 8$ to $n_\tau = 15$. The ΓM together with fits using `gnuplot` gives good results for meson masses with very small (relative) errors of only around 0.02% in the case of Fig. 4.1.

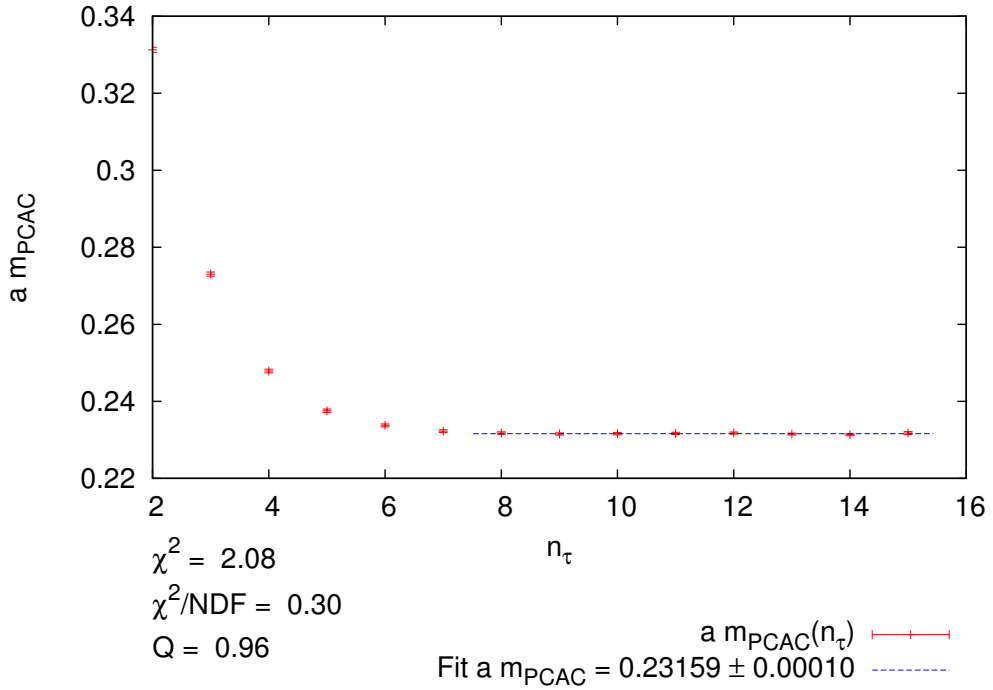

Figure 4.2.: PCAC quark mass plot and fit at $(\beta, \kappa) = (5.2420, 0.1650)$.

4.2.4. The PCAC Quark Mass from the Γ-Method

In order to calculate am_{PCAC}, the AP-correlator as well as the pseudoscalar meson correlator have to be implemented. Since am_{PCAC} has to be constant at least for large n_τ and $\langle \tilde{P}^-(\mathbf{0}, n_\tau) P^+(0) \rangle = \langle \tilde{O}_\pi(\mathbf{0}, n_\tau) \bar{O}_\pi(0) \rangle$ follows a shifted hyperbolic cosine behavior (see (3.38)), one can conclude from (3.51) that $\partial_4 \langle \tilde{A}_4^-(\mathbf{0}, n_\tau) P^+(0) \rangle$ also has to follow this behavior. Because of the derivative, $C(n_\tau) \coloneqq \langle \tilde{A}_4^-(\mathbf{0}, n_\tau) P^+(0) \rangle = -\langle \tilde{A}_4^-(\mathbf{0}, N_\tau - n_\tau) P^+(0) \rangle =: -C(N_\tau - n_\tau)$ must hold for the AP-correlator. Therefore, the correlator results from the HMC calculation can be pre-averaged replacing $C(n_\tau)$ with $(C(n_\tau) - C(N_\tau - n_\tau))/2$ for $0 < n_\tau < N_\tau/2$ for even N_τ. $C(0)$ and $C(N_\tau/2)$ stay the same as before.

The pseudoscalar meson correlator gets pre-averaged and replaced by its absolute value as described in Sect. 4.2.3. As for the pseudoscalar meson correlator, $C(n_\tau)$ gets replaced by $|C(n_\tau)|$ for all $0 \leq n_\tau \leq N_\tau/2$ to ensure that $am_{\mathrm{PCAC}} > 0$, since there is a possible minus sign for γ_4 depending on the convention and $|C(n_\tau)|$ is strictly monotonically decreasing for $0 \leq n_\tau \leq N_\tau/2$ because of the hyperbolic sine behavior.

Eq. (3.52) has been implemented as a function into `Matlab`, where the left-hand side of (3.52) is in fact $am_{\mathrm{PCAC}}(n_\tau)$, so that it can be passed as `fun` to the ΓM, thus calculating am_{PCAC} for every $0 < n_\tau < N_\tau/2$ using the pre-averaged correlators from the HMC calculation.

As stated in Sect. 3.3, (3.51) and (3.52) are strictly speaking only valid for $N_\tau, n_\tau \to \infty$ as for the effective mass. The limit $N_\tau \to \infty$ is approximated by $N_\tau \approx 2N_\sigma$, whereas the limit $n_\tau \to \infty$ manifests itself in the simulation with $am_{\mathrm{PCAC}}(n_\tau)$ becoming constant for large n_τ, but still $N_\tau \gg n_\tau$. Therefore, one can find the true PCAC quark mass am_{PCAC}

by plotting $am_{\mathrm{PCAC}}(n_\tau)$ against n_τ and fitting it similar to meson masses using `gnuplot`. An example plot and fit for the PCAC quark mass at $(\beta, \kappa) = (5.2420, 0.1650)$ can be found in Fig. 4.2. As for the meson mass in Fig. 4.1, $am_{\mathrm{PCAC}}(n_\tau)$ hits a plateau at a distance of $n_\tau = 8$ from the source to the sink and it can be fitted from $n_\tau = 8$ to $n_\tau = 15$. This gives good results for PCAC quark masses with very small (relative) errors of only around 0.04% in the case of Fig. 4.2.

5. Implementation in CL^{2}QCD

This chapter will give an introduction to the LQCD program used in this thesis, CL^{2}QCD, and describe the implementation of correlators.

5.1. Description of CL^{2}QCD

All simulations in this thesis were performed with CL^{2}QCD[1], a LQCD program based on OpenCL[2]. Therefore, it is able to use both, CPUs and GPUs, which are particularly well suited for LQCD, efficiently and achieves very good performance. CL^{2}QCD was developed by Dr. Matthias Bach, Dr. Christopher Pinke, and others [Phi+14].

An OpenCL program consists of a host program which executes the OpenCL functions, so-called kernels. The host program of CL^{2}QCD is written in `C++11` and contains the algorithm logic, parameter handling and similar functionality, whereas the OpenCL kernels do the actual calculations in the simulations [see Pin14, pp. 43, 53]. An example for an OpenCL kernel is a meson correlator. The executables of CL^{2}QCD used in this thesis are `hmc`, which was used to create gauge configurations using a HMC algorithm, and `inverter`, which was used to evaluate the correlators on the gauge configurations. CL^{2}QCD has the CG and the Bi-CGStab Krylov solvers implemented. More detailed information on CL^{2}QCD can be found in [Pin14] and [Phi+14].

5.2. Implementation of Correlators

There are three correlators of interest in this thesis: the pseudoscalar (pion) and vector (ρ) meson correlators and the PCAC correlator, for which the AP- and the pseudoscalar meson correlator have to be implemented and calculated. Meson correlators for the scalar, pseudoscalar, vector and axial vector (with $C = -1$) mesons had already been implemented at the beginning of this thesis using an even number of γ-matrices different from γ_5 for twisted mass fermions and can therefore be used with pure Wilson fermions (cf. Sect. 3.1.4). The only correlator that had to be implemented newly in CL^{2}QCD was the AP-correlator. However, in the work of this thesis, all correlator implementations got restructured and optimized. Since test-driven development [Bec02] is being used in the working group, tests for all meson correlators as well as the AP-correlator have been constructed and implemented.

Depending on their explicit structure, i.e. if the different spin components for the source mix, correlators can be calculated spin-color-, i.e. for fixed spin and color index of the source in the quark propagator in the calculation in the kernel, or color-wise, i.e. for fixed color index of the source in the quark propagator in the kernel. This means that for a spin-color-wise computation only one column with 12 entries of the complete propagator is passed to the kernel and for a color-wise computation 4 columns are passed to the kernel.

[1] CL^{2}QCD is available as a git through `https://github.com/CL2QCD/cl2qcd`.
[2] `https://www.khronos.org/opencl/`

The fixed indices are summed over by executing the kernel for every value they can assume and summing the result. The pseudoscalar meson correlator and the AP-correlator are calculated spin-color-wise, whereas all components of the vector and axial vector meson correlators as well as the scalar meson correlator are calculated color-wise.

In test-driven development, implementations are done while constantly writing tests. In order to be able to do so, a `Mathematica` notebook has been written that enables the calculation of the correlators for a given test matrix as a quark propagator spin-color- or color-wise depending on the correlator. Using these results and `Boost`[3], different tests for all correlators have been implemented in CL²QCD.

The actual calculation of the correlators in an OpenCL kernel can be summarized by Algorithm 1, where $C(n_\tau)$ is the meson correlator with fixed spin-color- or color-index of the source after fourier transformation and $c(n_1, n_2, n_3, n_\tau)$ is the meson correlator with fixed spin-color or color index of the source according to (3.23), (3.29), (3.30), (3.31) and (3.55):

Algorithm 1 Correlator calculation in an OpenCL kernel.

Input: $D^{-1}(n|m_0)$ for point source m_0 with fixed spin-color or color index
Output: $C(n_\tau)\ \forall\ 0 \leq n_\tau \leq N_\tau - 1$

```
for 0 ≤ n_τ ≤ N_τ − 1 do C(n_τ) = 0
    for 0 ≤ n_1, n_2, n_3 ≤ N_σ − 1 do
        Calculate c(n_1, n_2, n_3, n_τ)
        C(n_τ) ← C(n_τ) + c(n_1, n_2, n_3, n_τ)
    end for
    C(n_τ) ← C(n_τ) · 4κ²/N_σ³
end for
```

The factor $4\kappa^2$ comes from the rescaling of the fields (2.26) and the Dirac operator (2.27) and the division by N_σ^3 comes from the Fourier transformation. $C(n_\tau)$ then gets calculated for all values of the fixed indices. The results are added and given as the output for the correlator.

After all correlator kernels have been implemented and successfully tested, they can be used by the executable `inverter` to calculate the correlators on gauge configurations created using the executable `hmc`. The executable `inverter` writes all correlators into a single output file. The quantum numbers in this file indicate the meson described by the correlator and, for the AP-correlator, the quantum numbers for the axial vector and the pseudoscalar meson are given.

The complete procedure for the correlator implementation can be summarized by two steps. One first calculates the fermionic part of the expectation value analytically and projects the correlator to zero momentum. Afterwards, one implements the analytic result for spin-color- or color-wise calculation in OpenCL kernels with test-driven development. This implementation may be used to calculate the total correlator and extract the meson or PCAC quark masses for given simulation parameters according to the procedure given in Sect. 6.1.

[3] `http://www.boost.org`

6. Simulations

In this chapter, the simulation procedure will be explained and the results of the simulations, which were performed in the course of this thesis, will be presented and discussed.

6.1. Procedure

All simulations have been performed with $N_\sigma = 16$ and $N_\tau = 32$, i.e. a lattice of size $16^3 \times 32$, on GPU nodes on LOEWE-CSC[1] and L-CSC[2] using CL^{2}QCD. Each node provides four GPUs and therefore, there was a multiple of four Markov chains in the production of the gauge configurations in each simulation. The simulation details for all simulations can be found in Table A.1. The procedure of calculating the pion and ρ-meson mass as well as the PCAC quark mass for given lattice parameters (β, κ) can be summarized by the following steps:

1. Create gauge configurations using the executable `hmc`.
   a) Thermalize from hot with ~ 1000 HMC steps.
   b) Tune acceptance rate to $70\% \leq P_{\text{acc}} \leq 80\%$.
   c) Produce gauge configurations for evaluation of correlators.
      i. Use different PRNG seeds to run multiple Markov chains concurrently.
      ii. Save gauge configuration every 50 steps in each Markov chain.
2. Evaluate correlators on gauge configurations using the executable `inverter`.
   a) Use eight sources per gauge configuration placed on different random positions and average the result.
3. Extract masses from correlators using ΓM.
4. Fit mass curves using `gnuplot`.

The gauge configurations were created by Dr. Christopher Pinke and the author of this thesis (see Table A.1). The calculation of the correlators and the analyses of the results were performed only by the author of this thesis.

The calculation of the critical value of $\kappa_c(\beta)$ for a given β can be done with the following steps:

1. Roughly estimate $\kappa_c(\beta)$ using a fit/interpolation of literature values.
2. Calculate am_π, am_{PCAC} and am_ρ at increasing values of κ with the same β, thus reaching the regime, where these masses are small. Use am_ρ to set approximate scale and m_π/m_ρ as a guidance value to see when the chiral limit is approached.

[1] `https://csc.uni-frankfurt.de/index.php?id=loewe-hw`
[2] `http://www.green500.org/sites/default/files/SC14-bof-lcsc.pdf`

3. Plot $(am_\pi)^2$ and am_{PCAC} with their errors against $1/\kappa$.

4. Fit $(am_\pi)^2$ and am_{PCAC} to a linear function in the region where they are (approximately) linear to find $\kappa_c(\beta)$.

5. If χ^2/N_{DOF} and Q of the linear fit indicate non-linear contributions estimate the systematic error in $\kappa_c(\beta)$ using further quadratic fits, which usually give a lower error, and linear fits at masses that are not the smallest ones measured, which usually give an upper error.

6.2. Results

6.2.1. Verification of Procedure

In order to make sure all parts of the programs work, the first simulations were performed recalculating the results of [Eic+99] for pion and ρ-meson masses. The chiral extrapolation here was done for the PCAC quark mass and the pion mass to cross-check both procedures, whereas in [Eic+99] it was done only for the pion mass. Because of high computational expenses, only simulations for $\kappa = 0.1560, 0.1565, 0.1570$ and not for $\kappa = 0.1575$ have been performed. All simulations used $\beta = 5.6$. More details can be found in Table A.1. The simulation results can be found in Table 6.1.

κ	n_{conf}	am_π	Fit	Reference value
0.1560	142	0.44844(77)	$(12, 15)$	0.4452^{+32}_{-29}
0.1565	105	0.39546(109)	$(11, 15)$	0.4016^{+52}_{-50}
0.1570	145	0.34828(122)	$(11, 15)$	0.3486^{+49}_{-41}

κ	am_ρ	Fit	Reference value
0.1560	0.53616(106)	$(12, 15)$	0.5345^{+54}_{-49}
0.1565	0.48865(142)	$(11, 15)$	0.4966^{+70}_{-69}
0.1570	0.46525(199)	$(11, 15)$	0.4600^{+70}_{-72}

κ	m_π/m_ρ	Reference value	am_{PCAC}	Fit
0.1560	0.8364(22)	0.833(5)	0.067250(114)	$(8, 15)$
0.1565	0.8093(33)	0.809(15)	0.053795(130)	$(7, 15)$
0.1570	0.7486(42)	0.758(11)	0.041200(112)	$(8, 15)$

Table 6.1.: Simulation results for recalculation of [Eic+99], n_{conf} is the number of gauge configurations for the κ values for all correlators, reference value is the result from the paper and fit is the fit range. $0.11 \leq \chi^2/N_{\mathrm{DOF}} \leq 1.04$ and $0.38 \leq Q \leq 0.98$ was found for all fits.

As one can see from the simulation results, they agree with the results given in [Eic+99]. It is worth noting that, even though the simulations performed in this thesis have less than 198 gauge configurations, which was the number of configurations in [Eic+99], the errors

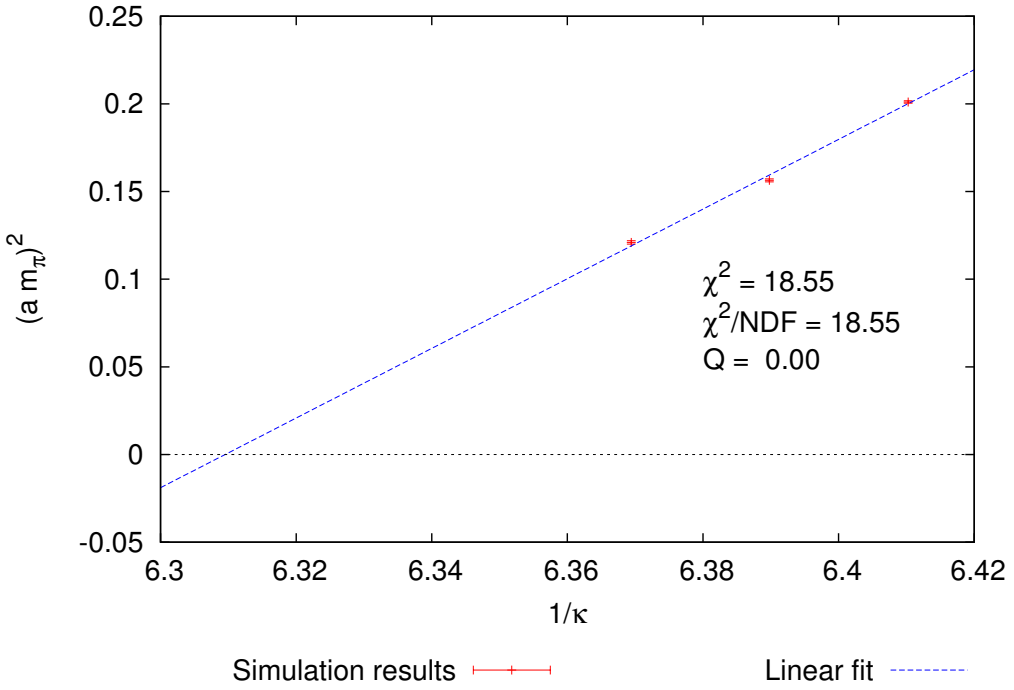

Figure 6.1.: Chiral extrapolation of $(am_\pi)^2$ for recalculation of [Eic+99], $\kappa_{c,\pi}(\beta = 5.6) = 0.158513(29)$.

here are smaller. One reason for this is autocorrelation, since firstly, every 25th trajectory was analyzed in [Eic+99] with autocorrelation times ranging from $\tau_{\text{int}} = 17(5)$ to $\tau_{\text{int}} = 33(22)$ and secondly, they have only been analyzed using blocking techniques. Apparently, the error estimation by the ΓM produces a better error. Autocorrelation times for these simulations range from $\tau_{\text{int}} = 0.31(7)$ to $\tau_{\text{int}} = 0.95(35)$ for every 50th configuration passed to the ΓM, i.e. $\tau_{\text{int}} = 16(4)$ to $\tau_{\text{int}} = 48(18)$ in time in the Markov chain. Since the upper limit is reached only at one n_τ for the pion mass at $\kappa = 0.1565$ in the fit range and all other values of $\tau_{\text{int}} < 1$ for the first timescale, one can say that autocorrelation does not play a very important role and was treated by the ΓM appropriately.

With these results one finds $\kappa_{c,\pi}(\beta = 5.6) = 0.158513(29)$ for the chiral extrapolation of $(am_\pi)^2$ (Fig. 6.1), whereas the value from the paper using all pion masses at κ =0.1560, 0.1565, 0.1570, 0.1575 is $\kappa_{c,\pi}(\beta = 5.6) = 0.158507^{+41}_{-44}$, and $\kappa_{c,q}(\beta = 5.6) = 0.158604(13)$ for the chiral extrapolation of am_{PCAC} (Fig. 6.2). Therefore, one can say that the values of the extrapolations of $(am_\pi)^2$ agree within their errors and, since the result from the extrapolation of am_{PCAC} is very close to the value, the cross-check confirms the result, even though it is not directly within the error from the fit. The fact that $\chi^2/N_{\text{DOF}} = 18.55$, $Q = 0$ for the chiral extrapolation of $(am_\pi)^2$ and $\chi^2/N_{\text{DOF}} = 6.48$, $Q = 0.01$ for the chiral extrapolation of am_{PCAC} is induced by the small errors in the masses from the ΓM and the fits of the mass curves. However, since the results of these simulations agree with the results from [Eic+99] within their errors, one can say that all parts of the programs work and the systematic errors of the extrapolations do not need to be analyzed.

Using $m_\rho = 775.26(25)$MeV to set the scale one finds estimates of m_π and m_{PCAC} given

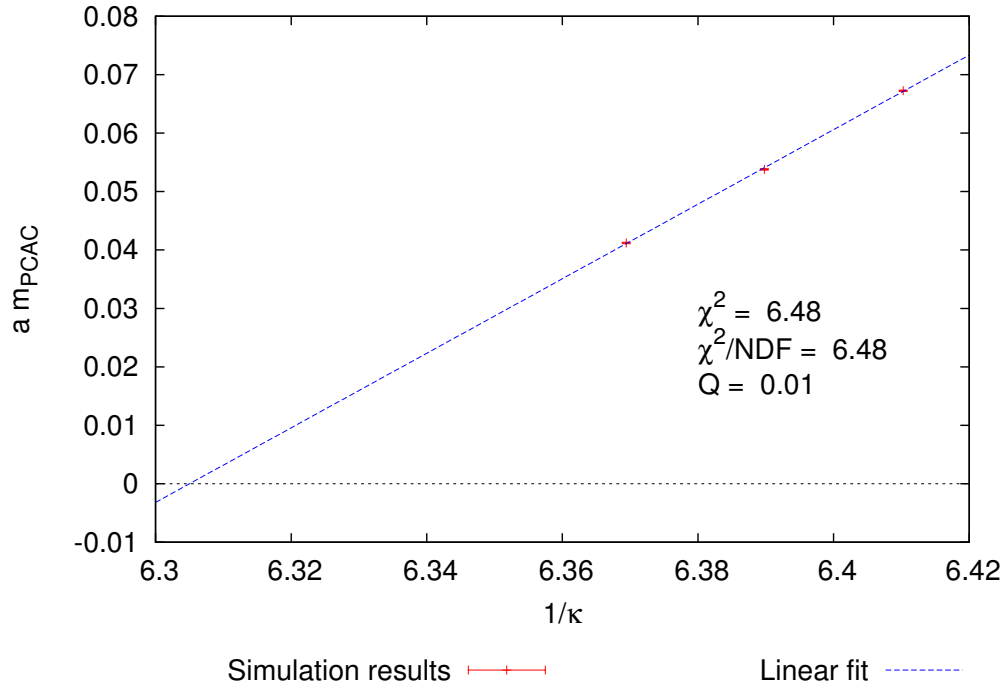

Figure 6.2.: Chiral extrapolation of am_{PCAC} for recalculation of [Eic+99], $\kappa_{c,q}(\beta = 5.6) = 0.158604(13)$.

in Table 6.2. Together with the values for m_π/m_ρ from Table 6.1 one can see that the simulations in fact were performed at heavy pion and quark masses far away from the chiral limit. This contributes to a (systematic) error on $\kappa_c(\beta = 5.6)$.

κ	a [fm]	m_π [MeV]	m_{PCAC} [MeV]
0.1560	0.13647(28)	648.4(18)	97.24(17)
0.1565	0.12437(37)	627.4(25)	85.35(21)
0.1570	0.11842(51)	580.3(33)	68.65(19)

Table 6.2.: Simulation results in physical units, where $m_\pi = 648.4(18)$ MeV means $m_\pi = (648.4 \pm 1.8)$ MeV.

6.2.2. Pion Masses Along the Chiral Critical Line

In order to relate LQCD simulations concerning the chiral phase transition and the chiral critical line to the point of simulation in the QCD phase diagram, pion masses were needed by the IMuP for the simulation parameters $(\beta, \kappa) = (5.2420, 0.1650)$, $(5.1500, 0.1700)$, $(5.0519, 0.1750)$, $(4.9519, 0.1800)$. These simulation points lie on the chiral critical line in the $N_f = 2$ QCD phase diagram for specific values of the chemical potential. The exact simulation details can be found in Table A.1. The results for am_π and am_ρ can be found in Table 6.3. Autocorrelation times in the fit ranges assume values from $\tau_{\mathrm{int}} = 0.35(9)$ to $\tau_{\mathrm{int}} = 1.08(46)$ with most being around $\tau_{\mathrm{int}} \approx 0.6$ in a scale, where 50 steps in the Markov

chains is a time of 1. Therefore, it can be assumed that autocorrelation has been treated appropriately by analyzing every 50th configuration with the ΓM.

(β, κ)	n_{conf}	am_π	Fit	am_ρ	Fit
$(5.2420, 0.1650)$	372	1.04213(22)	$(8, 15)$	1.14622(45)	$(8, 15)$
$(5.1500, 0.1700)$	400	1.00586(22)	$(8, 15)$	1.13157(55)	$(9, 15)$
$(5.0519, 0.1750)$	400	0.96545(20)	$(8, 15)$	1.11678(60)	$(8, 15)$
$(4.9519, 0.1800)$	305	0.90764(42)	$(5, 15)$	1.09052(160)	$(7, 14)$

Table 6.3.: Simulation results for pion and ρ-meson masses. Fit always refers to the fit range of the mass to the left. $0.20 \leq \chi^2/N_{\text{DOF}} \leq 1.01$ and $0.42 \leq Q \leq 0.99$ for all fits.

The results for m_π/m_ρ and the scale setting methods, where the scale setting using m_ρ was done by the author of this thesis and the scale setting using w_0 was done by Dr. Christopher Pinke, can be found in Table 6.4 and Table 6.5. Already from these tables one can see that setting the scale using $m_\rho = 775.26(25)$ MeV is not very exact, since m_ρ does depend on the simulation parameters, which can be seen from Table 6.5. The fact that the lattice spacing a decreases for decreasing β in the scale setting using m_ρ, whereas it should in fact be increasing for decreasing β as for the scale setting using w_0 [cf. Pin14, p. 16], further supports the statement that using m_ρ for scale setting only gives a rough estimate. The scale setting using w_0 is much more accurate.

(β, κ)	m_π/m_ρ	a [fm]	m_π [MeV]
$(5.2420, 0.1650)$	0.90919(41)	0.29175(15)	704.86(39)
$(5.1500, 0.1700)$	0.88891(48)	0.28802(17)	689.13(43)
$(5.0519, 0.1750)$	0.86449(50)	0.28425(18)	670.21(45)
$(4.9519, 0.1800)$	0.83230(128)	0.27757(42)	645.25(102)

Table 6.4.: Simulation results with scale setting via $m_\rho = 775.26(25)$ MeV. Note that m_π/m_ρ does not depend on the scale setting and is only listed here as a guidance for the distance to the physical points.

(β, κ)	w_0/a	a [fm]	m_π [MeV]	m_ρ [MeV]
$(5.2420, 0.1650)$	0.64801(16)	0.27083(278)	759.30(780)	835.14(858)
$(5.1500, 0.1700)$	0.60973(10)	0.28783(295)	689.59(707)	775.77(796)
$(5.0519, 0.1750)$	0.58381(7)	0.30061(308)	633.74(649)	733.08(752)
$(4.9519, 0.1800)$	0.56738(5)	0.30932(317)	579.02(594)	695.68(720)

Table 6.5.: Simulation results with scale setting via w_0 [cf. Bor+12].

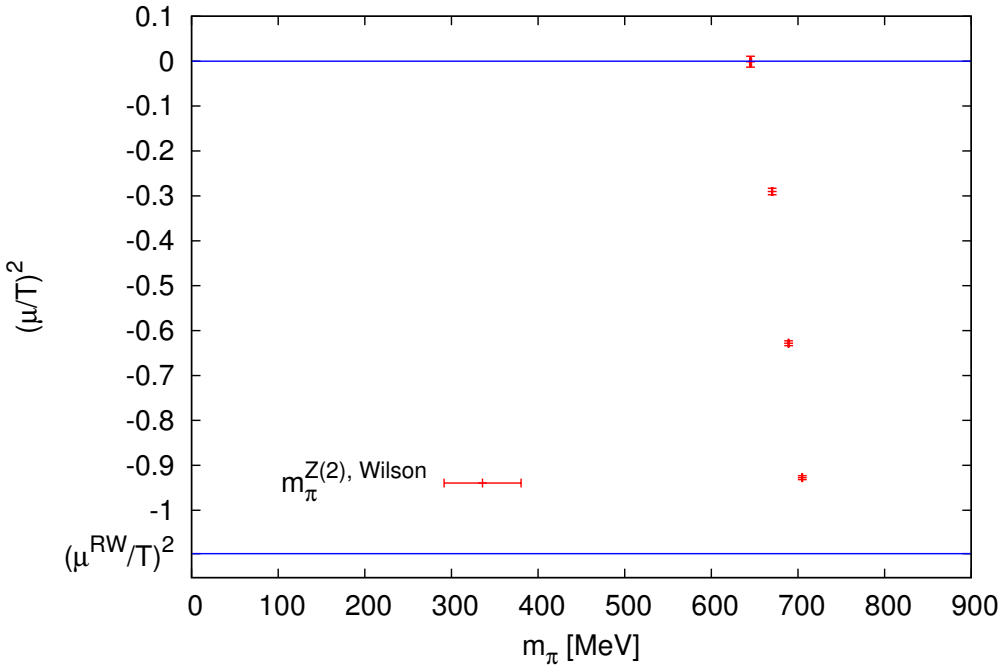

Figure 6.3.: Chiral phase transition in the $N_f = 2$ QCD phase diagram with m_π as x-axis using m_ρ scale setting.

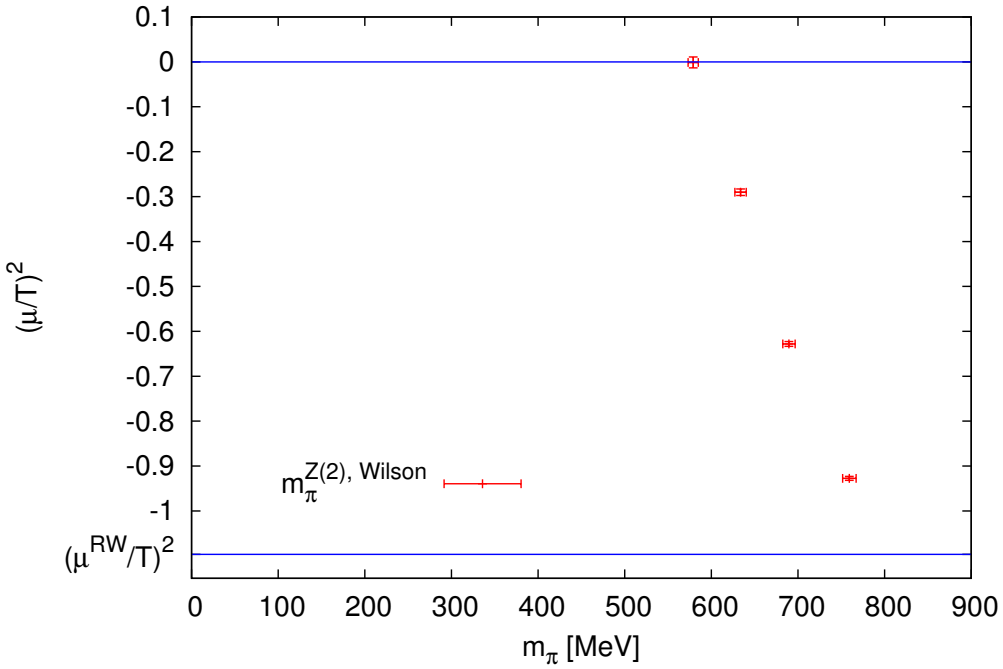

Figure 6.4.: Chiral phase transition in the $N_f = 2$ QCD phase diagram with m_π as x-axis using w_0 scale setting.

The plots for the chiral phase transition can now be made using m_π instead of κ as the x-axis. Since there are two possible scale settings, Fig. 6.3 is the one with the scale setting using m_ρ and Fig. 6.4 is the one with the scale setting using w_0. Note that $m_\pi^{Z(2),\text{Wilson}}$ are the pion masses from the simulations. As stated in the introduction, the values for $(\mu/T)^2$ for these points come from the IMuP and have been published in [PP15], in which the chiral phase transition is studied and where also the values for m_π from this thesis using w_0 for scale setting have been used. $(\mu^{\text{RW}}/T)^2 = -\pi^2/9$ is the Roberge-Weiss endpoint of the chiral phase transition [cf. Pin14, pp. 85-89]. The pion masses lie on the $Z(2)$ chiral critical line, where there is a second order chiral phase transition in the $N_f = 2$ QCD phase diagram. In the plot, to the left of the chiral critical there is a first order chiral phase transition and to the right of the plot there is a crossover chiral phase transition.

6.2.3. Chiral Extrapolations and Quark Masses Along the Chiral Critical Line

As it turned out in the course of this thesis, pion masses are sufficient to set the scale. This is because the simulation points do not lie within a scaling region around tricritical points at low masses in the QCD phase diagram (cf. Chapter 1), since pion masses along the chiral critical line for Wilson fermions and $N_\tau = 4$ range between 579(6) MeV and 759(8) MeV (cf. Table 6.4). Therefore, the quark masses have only been determined for $(\beta, \kappa) = (5.2420, 0.1650)$, $(5.1500, 0.1700)$, $(5.0519, 0.1750)$ using a chiral extrapolation. As a reference, a fit to a polynomial with a degree of 6 to literature values published between 1989 and 1998, since more recent studies could not be found in the range of β, was performed to interpolate between them by Dr. Christopher Pinke. Due to the age of the studies and the limited computational resources at that time, the errors are large. Besides, there were not many values of $\kappa_c(\beta)$ in the vicinity of the β values that are of interest in this thesis. Using (2.29) to calculate am_q and the scale-setting via w_0 from the simulations for the pion masses the estimates for $\kappa_c(\beta)$ and m_q can be found in Table 6.6. Note that, since it did not imply much more effort, also the value of $\kappa_c(\beta = 4.9519)$ and the quark mass at $(\beta, \kappa) = (4.9519, 0.1800)$ have been fitted.

(β, κ)	$\kappa_c(\beta)$	am_q	m_q [MeV]
$(5.2420, 0.1650)$	0.1705(16)	0.098(29)	72(21)
$(5.1500, 0.1700)$	0.1756(13)	0.094(22)	65(15)
$(5.0519, 0.1750)$	0.1822(8)	0.113(13)	74(8)
$(4.9519, 0.1800)$	0.1885(16)	0.125(24)	80(16)

Table 6.6.: Results for quark masses using a fit to literature values.

For the chiral extrapolations, there have been simulations performed at $0.1635 \leq \kappa \leq 0.1698$ for $\beta = 5.2420$, at $0.1700 \leq \kappa \leq 0.1743$ for $\beta = 5.1500$ and at $0.1750 \leq \kappa \leq 0.1788$ for $\beta = 4.9519$. The setup was a lattice with $N_\sigma = 16$ and $N_\tau = 32$ and every 50th configuration was used for correlator calculation. Exact simulation details can be found in Table A.1. The results for am_π and am_{PCAC} can be found in Tables 6.7, 6.8 and 6.9. Autocorrelation times range from $\tau_{\text{int}} = 0.34(6)$ to $\tau_{\text{int}} = 1.34(44)$ for $\beta = 5.2420$, from $\tau_{\text{int}} = 0.31(8)$ to $\tau_{\text{int}} = 1.88(66)$ for $\beta = 5.2420$ and from $\tau_{\text{int}} = 0.36(7)$ to $\tau_{\text{int}} = 0.92(28)$ for $\beta = 5.0519$ in the fit ranges with most around $\tau_{\text{int}} \approx 0.6$ in a timescale, where 50

steps in the Markov chain equal a time of 1, and the upper limits are only assumed rarely. Therefore, it can be said that autocorrelation was properly treated by only taking every 50th gauge configuration for analysis and using the ΓM for error estimation.

κ	n_{conf}	am_π	Fit	am_{PCAC}	Fit
0.1635	400	1.13037(21)	(8, 15)	0.27900(13)	(10, 15)
0.1640	400	1.10219(23)	(8, 15)	0.26335(11)	(8, 14)
0.1645	400	1.07275(22)	(8, 15)	0.24757(12)	(8, 13)
0.1650	372	1.04213(22)	(8, 15)	0.23159(10)	(8, 15)
0.1660	400	0.97067(26)	(8, 15)	0.19785(11)	(9, 15)
0.1680	400	0.77914(29)	(7, 15)	0.12394(10)	(9, 15)
0.1690	400	0.62392(38)	(7, 15)	0.079182(95)	(7, 15)
0.1693	320	0.55883(76)	(7, 15)	0.063632(174)	(7, 15)
0.1695	201	0.50013(74)	(7, 15)	0.051035(158)	(8, 15)
0.1698	329	0.37312(151)	(7, 15)	0.028796(210)	(7, 15)

Table 6.7.: Simulation results for pion and PCAC quark masses for chiral extrapolation at $\beta = 5.2420$. $0.13 \leq \chi^2/N_{\text{DOF}} \leq 1.20$ and $0.30 \leq Q \leq 1.00$ for all fits.

κ	n_{conf}	am_π	Fit	am_{PCAC}	Fit
0.1700	400	1.00586(22)	(8, 15)	0.20330(9)	(8, 15)
0.1705	400	0.97316(24)	(8, 15)	0.18817(10)	(9, 15)
0.1710	400	0.93671(24)	(9, 15)	0.17270(9)	(8, 15)
0.1715	400	0.89814(25)	(8, 15)	0.15684(10)	(9, 15)
0.1720	400	0.85373(25)	(8, 15)	0.14022(10)	(9, 14)
0.1730	400	0.74414(31)	(8, 15)	0.10391(11)	(9, 15)
0.1735	292	0.66249(61)	(7, 15)	0.081442(146)	(7, 15)
0.1740	183	0.54482(113)	(7, 15)	0.054651(229)	(7, 15)
0.1743	154	0.39652(155)	(6, 15)	0.028974(232)	(6, 15)

Table 6.8.: Simulation results for pion and PCAC quark masses for chiral extrapolation at $\beta = 5.1500$. $0.08 \leq \chi^2/N_{\text{DOF}} \leq 0.99$ and $0.44 \leq Q \leq 1.00$ for all fits.

κ	n_{conf}	am_π	Fit	am_{PCAC}	Fit
0.1750	400	0.96545(20)	(8, 15)	0.17663(8)	(8, 15)
0.1760	400	0.90130(19)	(6, 15)	0.15027(7)	(7, 15)
0.1770	400	0.82301(24)	(7, 15)	0.12203(8)	(7, 15)
0.1775	320	0.77500(36)	(7, 15)	0.10649(12)	(7, 15)
0.1780	400	0.71763(27)	(7, 15)	0.089723(75)	(7, 15)
0.1785	202	0.64099(46)	(6, 15)	0.070204(115)	(6, 15)
0.1788	320	0.57746(67)	(6, 15)	0.056235(153)	(7, 15)

Table 6.9.: Simulation results for pion and PCAC quark masses for chiral extrapolation at $\beta = 5.0519$. $0.20 \leq \chi^2/N_{\text{DOF}} \leq 0.63$ and $0.76 \leq Q \leq 0.99$ for all fits.

In order to give an idea of the distance to the physical point, am_ρ was measured, m_π/m_ρ was computed and $m_\rho = 775.26(25)$ MeV was used for scale setting. Note that the physical value of m_π/m_ρ is 0.180030(58). The results can be found in Tables 6.10, 6.11 and 6.12.

κ	am_ρ	Fit	m_π/m_ρ	a [fm]	m_π [MeV]	m_{PCAC} [MeV]
0.1635	1.22360(39)	(8, 15)	0.92381(35)	0.31144(15)	716.19(36)	176.77(9)
0.1640	1.19820(42)	(8, 15)	0.91987(38)	0.30498(15)	713.14(38)	170.39(8)
0.1645	1.17369(45)	(9, 15)	0.91400(40)	0.29874(15)	708.59(39)	163.53(8)
0.1650	1.14622(45)	(8, 15)	0.90919(41)	0.29175(15)	704.86(39)	156.64(7)
0.1660	1.08518(50)	(8, 15)	0.89448(48)	0.27621(16)	693.45(44)	141.35(8)
0.1680	0.92032(66)	(8, 15)	0.84660(69)	0.23425(19)	656.33(58)	104.40(9)
0.1690	0.79136(83)	(8, 15)	0.78841(96)	0.20142(23)	611.23(77)	77.57(10)
0.1693	0.73629(146)	(8, 15)	0.75898(183)	0.18741(38)	588.41(143)	67.00(19)
0.1695	0.69640(159)	(7, 15)	0.71816(196)	0.17725(41)	556.76(153)	56.81(18)
0.1698	0.60638(362)	(7, 15)	0.61532(444)	0.15434(93)	477.04(345)	36.82(27)

Table 6.10.: Simulation results in physical units for pion and PCAC quark masses at $\beta = 5.2420$. $0.22 \leq \chi^2/N_{\mathrm{DOF}} \leq 1.95$ and $0.06 \leq Q \leq 0.98$ for all fits for am_ρ.

κ	am_ρ	Fit	m_π/m_ρ	a [fm]	m_π [MeV]	m_{PCAC} [MeV]
0.1700	1.13157(55)	(9, 15)	0.88891(48)	0.28802(17)	689.13(43)	139.28(7)
0.1705	1.10563(53)	(8, 15)	0.88019(48)	0.28142(17)	682.37(43)	131.94(8)
0.1710	1.07534(62)	(9, 15)	0.87108(55)	0.27371(19)	675.32(48)	124.43(7)
0.1715	1.04378(57)	(7, 15)	0.86047(53)	0.26567(17)	667.09(47)	116.49(8)
0.1720	1.00545(75)	(9, 15)	0.84910(69)	0.25592(21)	658.28(57)	108.12(8)
0.1730	0.91839(85)	(8, 15)	0.81027(83)	0.23376(23)	628.17(67)	87.72(10)
0.1735	0.85369(155)	(7, 13)	0.77603(158)	0.21729(41)	601.63(124)	73.96(14)
0.1740	0.76777(226)	(7, 11)	0.70961(256)	0.19542(58)	550.14(199)	55.18(24)
0.1743	0.66393(451)	(6, 14)	0.59723(469)	0.16899(12)	463.01(364)	33.83(28)

Table 6.11.: Simulation results in physical units for pion and PCAC quark masses at $\beta = 5.1500$. $0.32 \leq \chi^2/N_{\mathrm{DOF}} \leq 1.13$ and $0.34 \leq Q \leq 0.93$ for all fits for am_ρ.

κ	am_ρ	Fit	m_π/m_ρ	a [fm]	m_π [MeV]	m_{PCAC} [MeV]
0.1750	1.11678(60)	(8, 15)	0.86449(50)	0.28425(18)	670.21(45)	122.62(6)
0.1760	1.06552(73)	(8, 15)	0.84588(61)	0.27121(21)	655.78(52)	109.33(6)
0.1770	1.00796(69)	(6, 15)	0.81651(61)	0.25656(20)	633.01(52)	93.86(7)
0.1775	0.96940(140)	(7, 15)	0.79946(122)	0.24674(37)	619.79(97)	85.16(10)
0.1780	0.92551(117)	(8, 14)	0.77539(103)	0.23557(31)	601.13(82)	75.16(7)
0.1785	0.86778(187)	(7, 12)	0.73865(168)	0.22088(49)	572.65(132)	62.72(11)
0.1788	0.82083(277)	(7, 15)	0.70351(252)	0.20893(71)	545.40(196)	53.11(15)

Table 6.12.: Simulation results in physical units for pion and PCAC quark masses at $\beta = 5.0519$. $0.25 \leq \chi^2/N_{\mathrm{DOF}} \leq 0.85$ and $0.52 \leq Q \leq 0.97$ for all fits for am_ρ.

Using these results, chiral extrapolations of $(am_\pi)^2$ and am_{PCAC} have been performed. Even using only the lowest three masses, linear fits had $\chi^2/N_{\mathrm{DOF}} \gg 1$ for all extrapolations. Consequently, the errors from the fits could not be used as errors for $\kappa_c(\beta)$ because of the systematic uncertainties mentioned in Sect. 2.3.1, while the results themselves could be used. Quadratic functions through the points with the three lowest masses have been calculated as part of the error analysis. Since the resulting $\kappa_c(\beta)$ was lower in all cases, the difference in the results were used as lower errors. One could also have used quadratic fits through the four points with the lowest masses, but this showed to produce smaller errors in all cases and therefore, the larger errors were used. For upper errors, linear functions through the points with the second and third smallest masses have been calculated and the difference of the resulting value for $\kappa_c(\beta)$, which was higher than the value for $\kappa_c(\beta)$ from the fit of three points in all extrapolations, were used as upper errors. The plots for $\beta = 5.2420$ can be found in Figs. 6.5 and 6.6. All other plots show the same behavior with the slope becoming monotonically smaller for higher values of $1/\kappa$ and are therefore not shown here. The results of the extrapolations can be found in Table 6.13.

	Extrapolation of $(am_\pi)^2$			Extrapolation of am_{PCAC}		
β	$\kappa_{c,\pi}(\beta)$	χ^2/N_{DOF}	Q	$\kappa_{c,q}(\beta)$	χ^2/N_{DOF}	Q
5.2420	0.170216^{+93}_{-101}	51.15	0.00	0.170225^{+90}_{-98}	43.28	0.00
5.1500	0.174812^{+242}_{-246}	534.22	0.00	0.174806^{+223}_{-238}	479.62	0.00
5.0519	0.180359^{+142}_{-568}	150.32	0.00	0.180215^{+106}_{-450}	90.20	0.00

Table 6.13.: Results for $\kappa_c(\beta)$. χ^2/N_{DOF} and Q refer to the linear fits using the 3 points with the lowest masses.

A comparison plot of the results for $\kappa_c(\beta)$ with the values obtained from the fit of literature values can be found in Fig. 6.7. All results have less errors than the predictions from the fit. For $\beta = 5.2420$ and 5.1500 the results are within the errors of the predictions. For $\beta = 5.0519$ the result is much lower than the prediction and not within the errors. However, the fact that the slope in the plots get monotonically smaller for higher $1/\kappa$, thus indicating a rapid decrease in mass when approaching $\kappa_c(\beta)$, supports the result for $\kappa_c(\beta = 5.0519)$ found in the course of this thesis. More simulations in the regions of small PCAC quark and pion masses would decrease the errors for all chiral extrapolations. Since the simulation expenses for the HMC algorithm get much larger in this region because of the inversion of the Dirac operator, which is more expensive for lower quark masses, a compromise had to be found and no more simulations were performed.

The results for the quark masses using (2.29) and the scale setting via m_ρ and w_0 from Sect. 6.2.2 can be found in Tables 6.14 and 6.15.

(β, κ)	m_q [MeV], m_ρ scale	m_q [MeV], w_0 scale
$(5.2420, 0.1650)$	$62.81^{+1.09}_{-1.18}$	$67.66^{+1.89}_{-1.95}$
$(5.1500, 0.1700)$	$55.47^{+2.71}_{-2.77}$	$55.50^{+3.32}_{-3.30}$
$(5.0519, 0.1750)$	$58.93^{+1.52}_{-6.08}$	$55.73^{+2.03}_{-6.26}$

Table 6.14.: Results for quark masses using the chiral extrapolation of $(am_\pi)^2$.

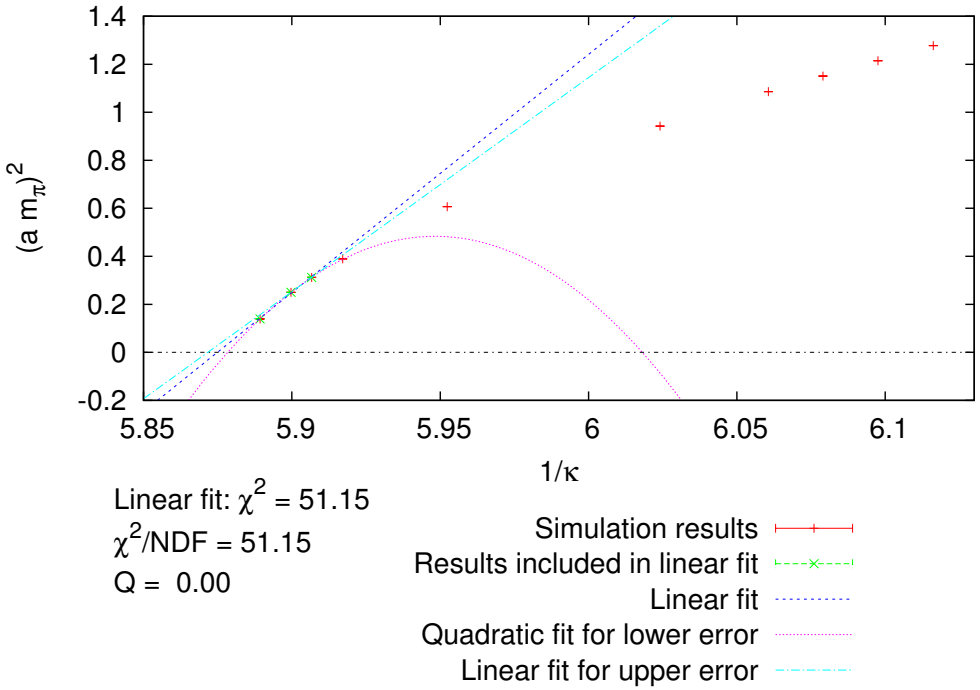

Figure 6.5.: Chiral extrapolation of $(am_\pi)^2$ for $\beta = 5.2420$, $\kappa_{c,\pi}(\beta = 5.2420) = 0.170216^{+93}_{-101}$.

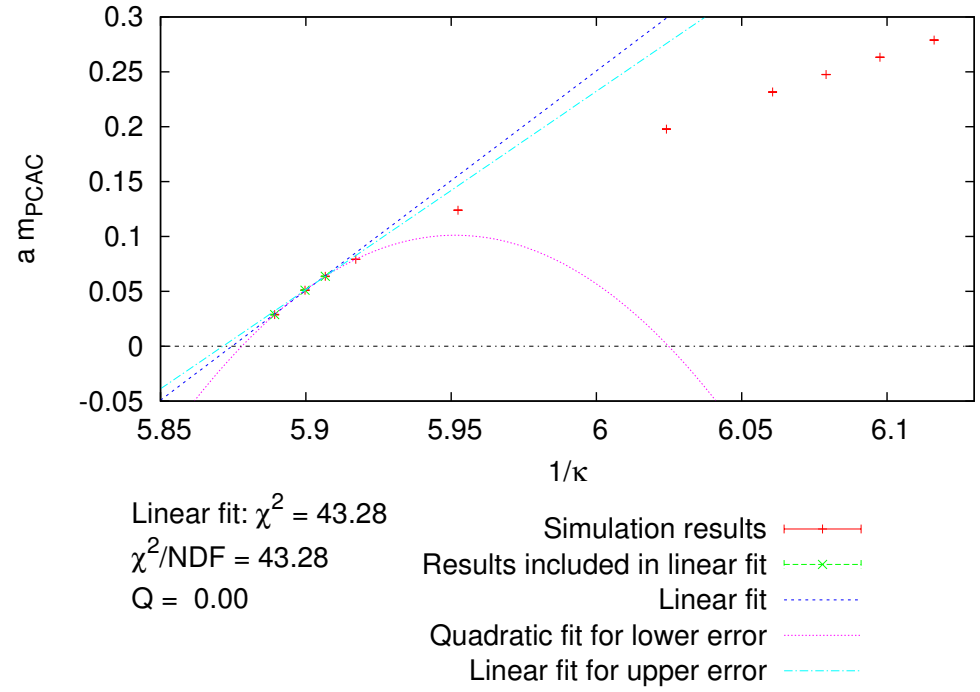

Figure 6.6.: Chiral extrapolation of am_{PCAC} for $\beta = 5.2420$, $\kappa_{c,q}(\beta = 5.2420) = 0.170225^{+90}_{-98}$.

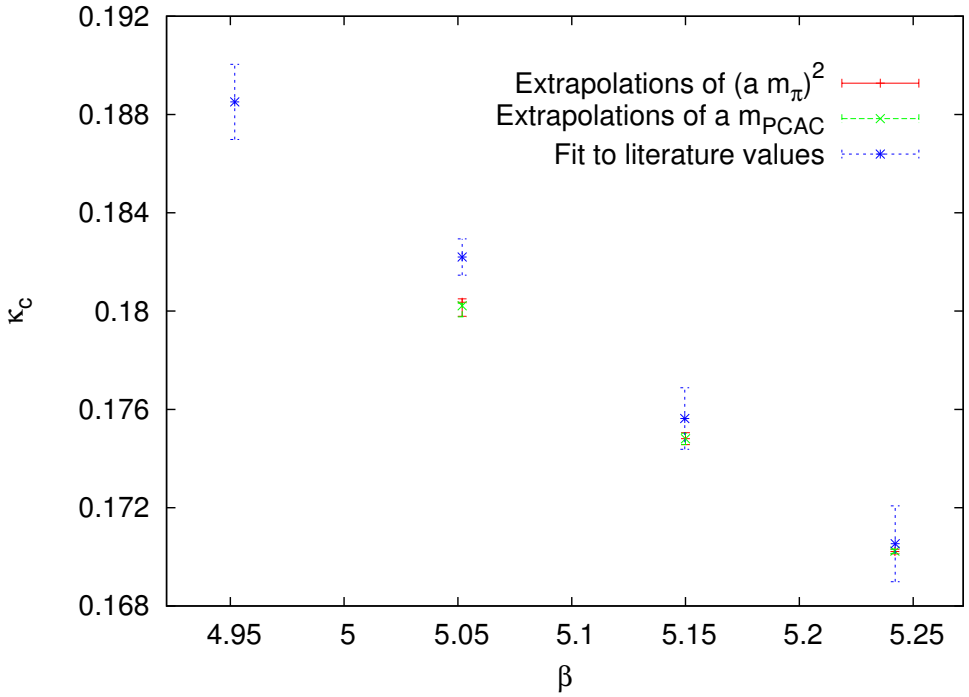

Figure 6.7.: Comparison of chiral extrapolation results with fit to literature values.

(β, κ)	m_q [MeV], m_ρ scale	m_q [MeV], w_0 scale
$(5.2420, 0.1650)$	$62.91^{+1.05}_{-1.15}$	$67.77^{+1.85}_{-1.91}$
$(5.1500, 0.1700)$	$55.40^{+2.50}_{-2.68}$	$55.44^{+3.10}_{-3.21}$
$(5.0519, 0.1750)$	$57.40^{+1.14}_{-4.83}$	$54.27^{+1.65}_{-5.07}$

Table 6.15.: Results for quark masses using the chiral extrapolation of am_{PCAC}.

Using these results, the plot for the chiral phase transition with the chiral critical line, Figs. 6.3 and 6.4, can be made with the quark mass as the x-axis. Again, there are two plots, one with the scale setting using m_ρ (Fig. 6.8) and one with the scale setting using w_0 (Fig. 6.9).

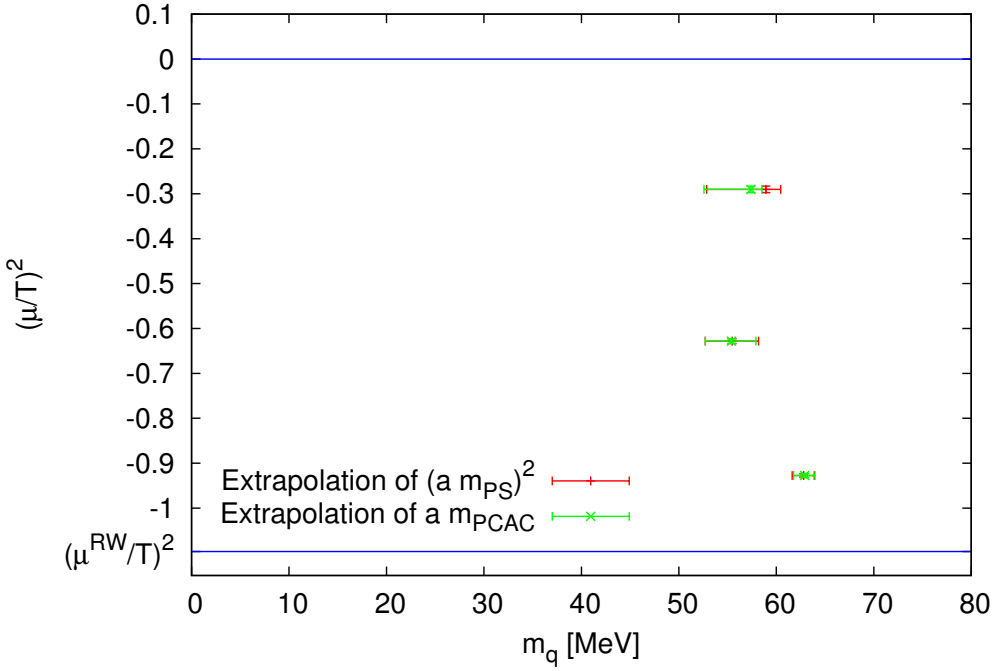

Figure 6.8.: Chiral phase transition in the $N_f = 2$ QCD phase diagram with m_q as x-axis using m_ρ scale setting.

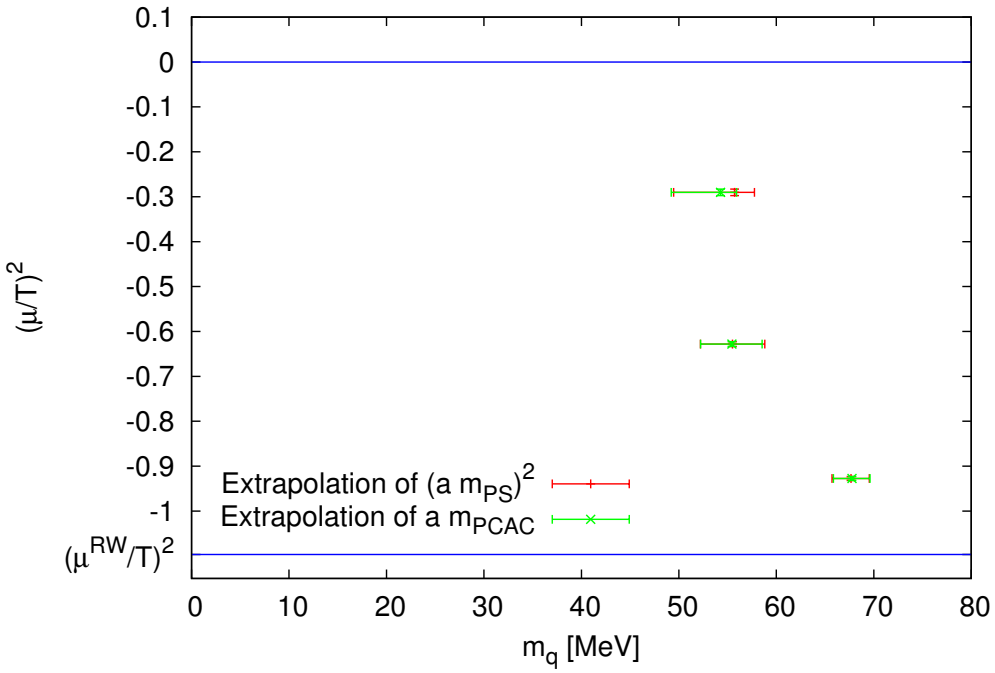

Figure 6.9.: Chiral phase transition in the $N_f = 2$ QCD phase diagram with m_q as x-axis using w_0 scale setting.

6.3. Discussion

After having reproduced the results from [Eic+99], it can be said that the simulation procedure and all programs work. Using the ΓM and fits as a method for the statistical analysis and mass extraction from the correlator results has proven to produce small errors while taking into account auto-correlation effects of the HMC algorithm.

The pion masses along the chiral critical line were determined with a relative error of around 1% for the more exact scale setting using w_0, which is a very high accuracy. In this context, it also needs to be said that even though the errors given in the Tables 6.4 and 6.5 are smaller for the m_ρ scale setting than for the w_0 scale setting, the error for the m_ρ scale setting only includes the uncertainty in $m_\rho = 775.26(25)$ MeV and in the simulation results for the masses. A systematic error coming from the fact that this method of setting the scale itself is not very exact is not included. Therefore, the results from the w_0 scale setting are much more reliable. They show that the pion mass decreases on the chiral critical line for Wilson fermions at $N_\tau = 4$ with increasing $(\mu/T)^2$.

The results for the quark masses from both chiral extrapolations agree very well within their errors. However, with relative errors ranging from 2.8% to 11.2% for the w_0 scale setting, they could not be determined with an accuracy as high as for the pion masses. This is because of the systematic errors in the chiral extrapolations due to non-linear terms contributing to $(am_\pi)^2$ and am_{PCAC}. Even though these contributions were found, chiral extrapolations with new simulations have proven to produce less and more controllable errors than a fit to literature values, especially since a lot of the reference studies are not recent.

Comparing the scale setting methods for the quark mass, one notices that for the scale setting using m_ρ, the quark mass at $(\beta, \kappa) = (5.1500, 0.1700)$ is lower than at $(\beta, \kappa) = (5.0519, 0.1750)$, which is unexpected as a lower bare quark mass should imply a lower (renormalized) quark mass. This is also the behavior in terms of the pion mass (cf. Table 6.5). However, using the scale setting via w_0, this problem is resolved and the quark mass at $\kappa = 0.1700$ is higher than at $\kappa = 0.1750$. It is worth noting that especially at $(\beta, \kappa) = (5.0519, 0.1750)$ the quark mass has a rather large lower error. A better estimate of $\kappa_c(\beta = 5.0519)$ could improve this and result in a lower quark mass at these parameters. This comparison of the scale setting methods shows that the one using w_0 is much more precise and gives better results as can be expected. Using this scale setting and the results for the quark masses, the chiral critical line in Fig. 6.9 agrees qualitatively with the chiral critical line in Fig. 6.4 with the pion and quark masses becoming smaller when going to larger $(\mu/T)^2$. It can therefore be said that pion and quark masses along the chiral critical line in the $N_f = 2$ QCD phase diagram were determined successfully giving consistent results. Even though the pion masses are sufficient as a scaling for the quark masses could not be applied, the quark masses still give a good cross-check for the results for the pion masses and confirm the results qualitatively.

In all plots for the chiral phase transition, there is a second order phase transition of universality class $Z(2)$ at the points drawn in the diagrams on the chiral critical line. To the left of this line there is a first order region for the chiral phase transition and to the right of this line there is a crossover region. This indicates a first order chiral phase transition in the $N_f = 2$ chiral limit $m_{u,d} = 0$, $m_\pi = 0$ at least for Wilson fermions on coarse $N_\tau = 4$ lattices.

7. Summary

In this thesis, pion and quark masses along the chiral critical line in the $N_f = 2$ Quantum Chromodynamics phase diagram have been calculated. To do so, after an introduction to QCD and lattice QCD, meson correlators, the effective mass and the PCAC quark mass with its corresponding correlators, have been introduced. In order to be able to calculate quark masses, the critical hopping parameter has been defined. The fermionic parts of the expectation values of the studied correlators have been calculated. An overview of the hybrid Monte Carlo algorithm for the simulation of the gauge part of the expectation values has been given together with the statistical methods for the analysis, where the Γ-method has been used, as well as the fits needed for the extraction of masses from the correlators. The LQCD program CL^{2}QCD and the implementation of correlators in it have been described. At last, the results of the simulations and, therefore, the pion and quark masses have been presented and discussed.

The results of this thesis were used by the Imaginary Chemical Potential Project in [PP15] to relate LQCD simulation parameters, which describe where the chiral critical line in the $N_f = 2$ QCD phase diagram at imaginary chemical potential is, to pion masses. They indicate that at least for Wilson fermions on coarse $N_\tau = 4$ lattices the chiral phase transition in the $N_f = 2$ chiral limit is of first order. Further studies of the chiral phase transition with higher values of $N_\tau > 4$, i.e. less coarse lattices, could enable a better comparison to continuum QCD and eventually, for high values of N_τ, a continuum extrapolation. However, such studies would require increasing computational effort.

As stated before, even though it turned out in the course of this thesis that the pion masses are sufficient, the determined quark masses offer a good cross-check. Besides, the values of the critical hopping parameter found enable the calculation of quark masses in future simulations, either directly or as an estimate by using them together with literature values in an interpolation to find $\kappa_c(\beta)$ at another value of β. Further simulations at high values of κ for the chiral extrapolations for smaller errors as well as a chiral extrapolation to find $\kappa_c(\beta = 4.9519)$ would improve these possibilities.

A. Appendix

A.1. Dirac and Pauli-Matrices

The conventions for the Euclidean Dirac matrices used in this thesis are:

$$\gamma_1 = \begin{pmatrix} 0 & 0 & 0 & -i \\ 0 & 0 & -i & 0 \\ 0 & i & 0 & 0 \\ i & 0 & 0 & 0 \end{pmatrix}, \ \gamma_2 = \begin{pmatrix} 0 & 0 & 0 & -1 \\ 0 & 0 & 1 & 0 \\ 0 & 1 & 0 & 0 \\ -1 & 0 & 0 & 0 \end{pmatrix}, \ \gamma_1 = \begin{pmatrix} 0 & 0 & -i & 0 \\ 0 & 0 & 0 & i \\ i & 0 & 0 & 0 \\ 0 & -i & 0 & 0 \end{pmatrix},$$

$$\gamma_4 = \begin{pmatrix} 0 & 0 & -1 & 0 \\ 0 & 0 & 0 & -1 \\ -1 & 0 & 0 & 0 \\ 0 & -1 & 0 & 0 \end{pmatrix}, \ \gamma_5 = \gamma_1\gamma_2\gamma_3\gamma_4 = \begin{pmatrix} -1 & 0 & 0 & 0 \\ 0 & -1 & 0 & 0 \\ 0 & 0 & 1 & 0 \\ 0 & 0 & 0 & 1 \end{pmatrix}. \tag{A.1}$$

Note that γ_4 and therefore also γ_5 differ from the conventions used in [GL10, pp. 330-331] by an overall minus sign. This, however, does not change the validity of the Euclidean anti-commutation relation

$$\{\gamma_\mu, \gamma_\nu\} = 2\delta_{\mu\nu}\mathbb{1}_{4\times4} \ , \tag{A.2}$$

the relations for the γ_5 matrix

$$\{\gamma_\mu, \gamma_5\} = 0, \ \gamma_5^2 = \mathbb{1}_{4\times4} \ , \tag{A.3}$$

the relation for the inverse

$$\gamma_\mu = \gamma_\mu^\dagger = \gamma_\mu^{-1} \ , \tag{A.4}$$

and the relation for charge conjugation

$$C\gamma_\mu C^{-1} = -\gamma_\mu^T \ , \tag{A.5}$$

where $\mu = 1, 2, 3, 4$ and C is the charge conjugation matrix, cf. Sect. 2.2.2. All these relations are taken from [GL10, pp. 330-331]. As it was shown in Sect. 2.2.2, one finds

$$C\gamma_5 C^{-1} = \gamma_5^T \ . \tag{A.6}$$

The conventions used for the Pauli matrices in this thesis are as in [GL10, p. 329]:

$$\sigma_1 = \tau^1 = \begin{pmatrix} 0 & 1 \\ 1 & 0 \end{pmatrix}, \ \sigma_2 = \tau^2 = \begin{pmatrix} 0 & -i \\ i & 0 \end{pmatrix}, \ \sigma_3 = \tau^3 = \begin{pmatrix} 1 & 0 \\ 0 & -1 \end{pmatrix}. \tag{A.7}$$

A.2. Simulation Details

All simulations were performed on lattices with $N_\sigma = 16$ and $N_\tau = 32$ using CL^{2}QCD and saving every 50th gauge configuration in the Markov chains for correlator calculation after thermalization. The correlators were calculated for 8 different random sources per gauge configuration giving the average as the result for each gauge configuration. All

HMC calculations have been tuned to an acceptance rate of $70\% \leq P_{\text{acc}} \leq 80\%$. The gauge configurations have been produced by Dr. Christopher Pinke and the author of this thesis on LOEWE-CSC and L-CSC, whereas all correlator calculations on the gauge configurations were done on LOEWE-CSC by the author of this thesis. The simulation details can be found below.

β	κ	τ_{therm}	n_{conf}	κ_{mp}	n_{chains}
5.6000	0.1560	1000	142	–	4
5.6000	0.1565	1000	105	–	4
5.6000	0.1570	850	145	–	4
5.2420	0.1635	1000	400	–	4
5.2420	0.1640	1000	400	–	4
5.2420	0.1645	1700	400	–	4
5.2420	0.1650	1700	372	–	4
5.2420	0.1660	1000	400	–	4
5.2420	0.1680	2000	400	–	4
5.2420	0.1690	1000	400	–	4
5.2420	0.1693	950	320	–	8
5.2420	0.1695	800	201	–	4
5.2420	0.1698	900	329	0.1640	8
5.1500	0.1700	1000	400	–	4
5.1500	0.1705	1000	400	–	4
5.1500	0.1710	1000	400	–	4
5.1500	0.1715	1200	400	–	4
5.1500	0.1720	1200	400	–	4
5.1500	0.1730	2000	400	–	4
5.1500	0.1735	1150	292	–	8
5.1500	0.1740	1000	183	–	4
5.1500	0.1743	900	154	0.1685	8
5.0519	0.1750	2000	400	–	4
5.0519	0.1760	2000	400	–	4
5.0519	0.1770	1600	400	–	4
5.0519	0.1775	1000	320	–	8
5.0519	0.1780	1050	400	–	4
5.0519	0.1785	1000	202	–	4
5.0519	0.1788	1000	320	0.1725	8
4.9519	0.1800	1000	305	–	16

Table A.1.: Simulation details.

In the table, τ_{therm} is the number of HMC thermalization steps, n_{conf} is the number of configurations for measurement, κ_{mp} is the κ value for mass preconditioning, where "–" indicates no mass preconditioning and n_{chains} is the number of Markov chains using different PRNG seeds in the creation of gauge configurations after thermalization.

Bibliography

[Bec02] Beck, K. (2002). *Test Driven Development: By Example*. Boston, MA, USA: Addison-Wesley Longman Publishing Co., Inc.

[Bor+12] Borsanyi, S. et al. (2012). "High-precision scale setting in lattice QCD". In: *JHEP* 09, p. 010. DOI: 10.1007/JHEP09(2012)010. arXiv: 1203.4469 [hep-lat].

[BS80] Bronstein, I. N. and Semendjajew, K. A. (1980). *Taschenbuch der Mathematik*. 19th Edition. Thun, Frankfurt/Main: Harri Deutsch.

[Eic+99] Eicker, N. et al. (1999). "Light and strange hadron spectroscopy with dynamical Wilson fermions". In: *Phys. Rev.* D59, p. 014509. DOI: 10.1103/PhysRevD.59.014509. arXiv: hep-lat/9806027 [hep-lat].

[GL10] Gattringer, C. and Lang, C. B. (2010). *Quantum Chromodynamics on the Lattice: An Introductory Presentation*. Lect. Notes Phys. 788. Berlin, Heidelberg: Springer.

[Has01] Hasenbusch, M. (2001). "Speeding up the hybrid Monte Carlo algorithm for dynamical fermions". In: *Phys. Lett.* B519, pp. 177–182. DOI: 10.1016/S0370-2693(01)01102-9. arXiv: hep-lat/0107019 [hep-lat].

[Iwa+96] Iwasaki, Y. et al. (1996). "Finite temperature transitions in lattice QCD with Wilson quarks: Chiral transitions and the influence of the strange quark". In: *Phys. Rev.* D54, pp. 7010–7031. DOI: 10.1103/PhysRevD.54.7010. arXiv: hep-lat/9605030 [hep-lat].

[Oli+14] Olive, K. A. et al. (2014). "Review of Particle Physics". In: *Chin. Phys.* C38, p. 090001. DOI: 10.1088/1674-1137/38/9/090001.

[Phi10] Philipsen, O. (2010). "Lattice QCD at non-zero temperature and baryon density". In: *Modern perspectives in lattice QCD: Quantum field theory and high performance computing. Proceedings, International School, 93rd Session, Les Houches, France, August 3-28, 2009*, pp. 273–330. arXiv: 1009.4089 [hep-lat].

[PP15] Philipsen, O. and Pinke, C. (2015). "The $N_f = 2$ chiral phase transition from imaginary chemical potential with Wilson Fermions". In: *Proceedings, 33rd International Symposium on Lattice Field Theory (Lattice 2015)*. arXiv: 1508.07725 [hep-lat].

[Phi+14] Philipsen, O. et al. (2014). "CL^{2}QCD - Lattice QCD based on OpenCL". In: *PoS* LATTICE2014, p. 038. arXiv: 1411.5219 [hep-lat].

[Pin14] Pinke, C. (2014). "Lattice QCD at Finite Temperature with Wilson Fermions". Ph.D. Thesis. Goethe-Universität Frankfurt/Main: Fachbereich Physik.

[SSV11] Schaefer, S. et al. (2011). "Critical slowing down and error analysis in lattice QCD simulations". In: *Nucl. Phys.* B845, pp. 93–119. DOI: 10.1016/j.nuclphysb.2010.11.020. arXiv: 1009.5228 [hep-lat].

[Td06] Takaishi, T. and de Forcrand, P. (2006). "Testing and tuning new symplectic integrators for hybrid Monte Carlo algorithm in lattice QCD". In: *Phys. Rev.* E73, p. 036706. DOI: 10.1103/PhysRevE.73.036706. arXiv: hep-lat/0505020 [hep-lat].

[Urb+06] Urbach, C. et al. (2006). "HMC algorithm with multiple time scale integration and mass preconditioning". In: *Comput. Phys. Commun.* 174, pp. 87–98. DOI: 10.1016/j.cpc.2005.08.006. arXiv: hep-lat/0506011 [hep-lat].

[Wol04] Wolff, U. (2004). "Monte Carlo errors with less errors". In: *Comput. Phys. Commun.* 156. [Erratum: Comput. Phys. Commun. 176 (2007), p. 383], pp. 143–153. DOI: 10.1016/S0010-4655(03)00467-3,10.1016/j.cpc.2006.12.001. arXiv: hep-lat/0306017 [hep-lat].

[You12] Young, P. (2012). "Everything you wanted to know about Data Analysis and Fitting but were afraid to ask". In: arXiv: 1210.3781 [physics.data-an].

Danksagung

Ich danke Professor Owe Philipsen für die Möglichkeit, in seiner Arbeitsgruppe diese Bachelorarbeit verfassen zu können. Auch für zahlreiche Beratungen, Hilfestellungen und stets offene Gespräche möchte ich mich bei ihm bedanken. Zudem danke ich Dr. Christopher Pinke für die vielen Hilfestellungen, sei es in theoretischen Teilen, beim Programmieren oder bei Simulationen, die er mir gegeben hat und die Zeit, die er dafür verwendet hat. Ohne diese Hilfe wäre diese Bachelorarbeit nicht möglich gewesen.

Selbstständigkeitserklärung

Erklärung nach § 30 (12) Ordnung für den Bachelor- und dem Masterstudiengang

Hiermit erkläre ich, dass ich die Arbeit selbstständig und ohne Benutzung anderer als der angegebenen Quellen und Hilfsmittel verfasst habe. Alle Stellen der Arbeit, die wörtlich oder sinngemäß aus Veröffentlichungen oder aus anderen fremden Texten entnommen wurden, sind von mir als solche kenntlich gemacht worden. Ferner erkläre ich, dass die Arbeit nicht - auch nicht auszugsweise - für eine andere Prüfung verwendet wurde.

Frankfurt am Main, den 17. September 2015

Paul Frederik Depta